Reply to referee comments

We would like to thank the two referees for their constructive comments, which helped us to improve the manuscript. The specific comments (highlighted in blue font) are shown below with our replies (normal text).

One issue that both referees raise is that other SIP mechanism (droplet shattering and ice-ice collisional breakup) used in our previous study (Calderón et al.: Secondary ice formation in cumulus congestus clouds: insights from observations and aerosol-aware large-eddy simulations, *Atmos. Chem. Phys.*, 25, 14479-14500, https://doi.org/10.5194/acp-25-14479-2025, 2025.) were excluded. In this study, we employed another model version that did not include the other SIP processes (but includes the Seifert and Beheng (SB) microphysics). Also, the temperature range and the absence of large droplets pointed towards rime splintering. Nevertheless, we have now implemented the missing ice-ice collisional breakup (IIBR) and droplet shattering (DS) processes to our SALSA version and repeated the simulations (please, see the revised manuscript). As expected, (1) rime splintering is the dominating SIP process and (2) including the other SIP processes does not change model predictions significantly, so our conclusions are valid.

Figure 1 shows results from the revised (default setup and RS multiplied by one and ten) and previous (RS multiplied by ten; no other SIP processes) model versions. Clearly RS is about three orders of magnitude stronger than the other processes. In addition, rime splintering production rates as well as ice crystal number concentrations (ICNCs) from the original and new RSx10 simulations are practically indistinguishable, which means that the other two SIP processes are insignificant. We have also verified that RS, IIBR and DS SIP rates are similar for the other two INP concentrations (1 and 10 kg^{-1}).

The manuscript is updated so that previously missing SIP processes are now described briefly and their impact on ice concentrations is quantified. All SALSA results (figures and tables) have been updated, because they now account for the three SIP processes, but they have no impact on our conclusions. Results based on the Seifert and Beheng (SB) microphysics have not changed.

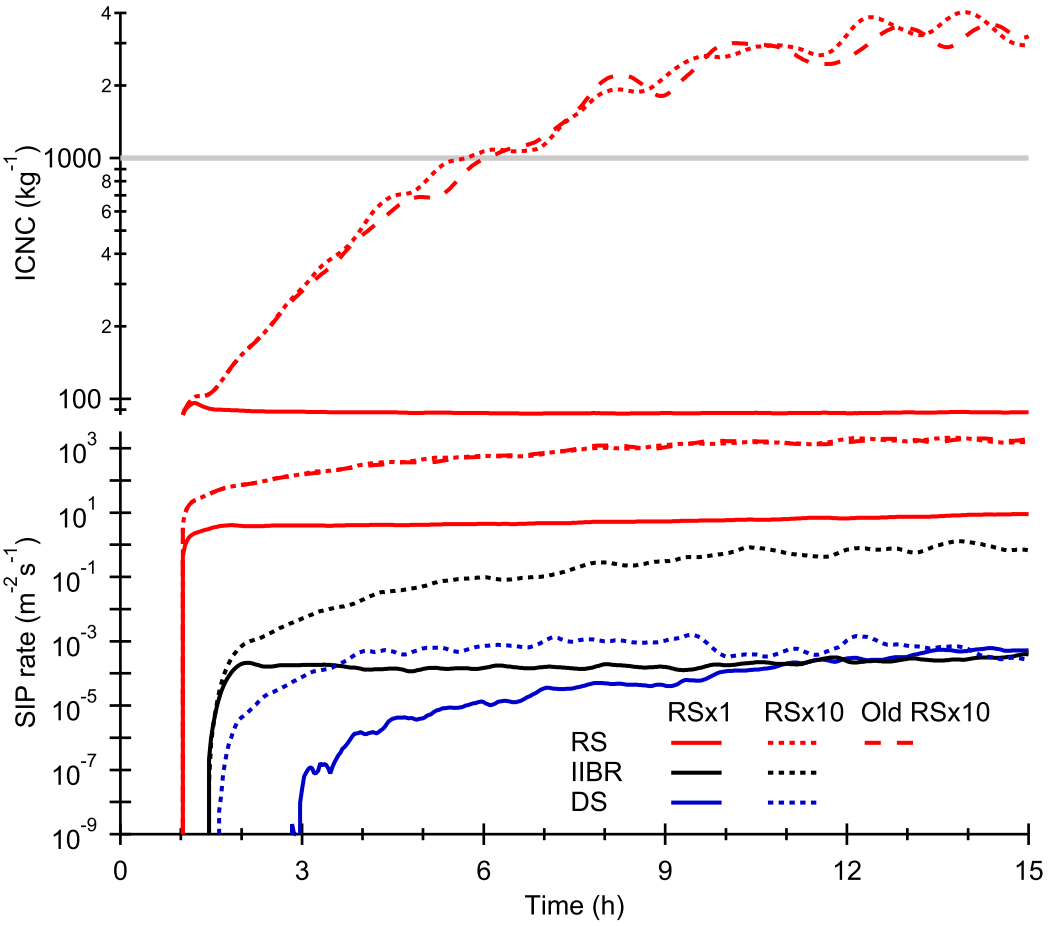

Figure 1: Ice crystal number concentrations (ICNCs) and secondary ice production (SIP) rates from UCLALES-SALSA simulations with INP concentration of 100 kg^{-1} and different multiplication factors for the rime splintering (RS) process. The last simulation is from the old manuscript where RS is the only SIP process. The thick gray line shows the target minimum ICNC of 1000 kg^{-1}.

Referee #1

REVIEW FOR RAATIKAINEN ET AL.

This modeling study examines whether the Hallett Mossop process can explain the high ICNCs observed within an Arctic stratocumulus deck during ACLOUD campaign, using LES simulations. Their results show that the current widely-used parameterization for the Hallett-Mossop mechanism cannot reproduce observations, unless its efficiency is enhanced by factor of ten. Alternatively, other microphysical formulations (e.g. terminal velocity calculation or HM temperature efficiency) should be modified in certain ways that can positively impact ice production from this process, to achieve a realistic ICNC representation.

The large discrepancies between INP-ICNC observations in Arctic clouds have been documented for a long time, with SIP being hypothesized as the potential cause. However, atmospheric models still struggle to reproduce the microphysical structure of Arctic clouds, even when SIP parameterizations are accounted for. This is largely due to the fact that SIP descriptions remain highly uncertain, which is why sensitivity studies like this one are very useful for the cloud modeling community.

Overall, I find the design of the study and the sensitivity tests satisfying, however I believe that results are not properly discussed. For example, while observations of micro- and macro-physical properties are available, they are not used for evaluation of e.g. different schemes or different HM formulations. Moreover, there is hardly any discussion on the differences in using different microphysical schemes (these sensitivity tests are neither discussed in the abstract nor in the conclusion section). I also think there some inconsistencies between the background information provided in this study and the relevant papers that are cited as reference.

A more detailed list of comments is given below. I don't think it would take a long time to the authors to address these - for this reason I consider the suggested revisions as minor.

Main comments:

Line 10: ' SIP depends strongly on model parametrizations', this is a very generalized statement (and not anything new). Should become more specific on what kind of parameterizations you refer to

Changed to 'SIP depends strongly on model parametrizations (e.g., fall velocity–mass–dimension parametrizations and those describing the dependency of SIP on temperature and particle size and habit)'.

Line 14: 'cooler marine regions', cooler than what

Changed cooler to high-latitude.

Line 20: 'simplified cloud microphysics.' Could you provide reference? I do not necessarily agree. I think two-moment fully prognostic schemes are rather complex

We removed 'simplified cloud microphysics' because low resolution alone is enough.

Line 32: 'The process is effective at cooler temperatures around -15°C'. Takahashi et al. (1995) with a rather unrealistic set-up showed maximum efficiency round -15°C. However, numerous more recent studies have shown that this process can be active over a much wider temperature range

We will clarify that the maximum efficiency is close to that temperature. We will also add simulations (please, see the beginning of this reply and the revised manuscript) where the three SIP processes are included to show that rime splintering is the dominant process in our case.

Line 34: Not true. Figure 7 in Keinert et al (2020) shows that the process can be effective above - 10°C. It is more effective below this temperature

Keinert et al. (2020) and the above -10 °C temperatures are already mentioned just below that line. As mentioned above, we tested the effectiveness of droplet shattering SIP.

Line 187-189: What was the criteria for adjusting surface fluxes and subsidence? These choices can have a large impact on the simulated LWP/TWP.

As mentioned in the text, we did simulations where the fluxes were calculated based on surface temperature (close to freezing point of sea water) and RH=100 % at the surface. The fixed surface flux values are based on those simulations. Divergence 5e-6 s^{-1} may sound quite high, but for the low clouds in this study it means modest vertical velocity of about 2.5 mm/s at the cloud top (500 m altitude). Based on several test simulations, this value was found to be large enough to limit the increase in LWP in simulations with low ice concentration (less precipitation) and, on the other hand, low enough to maintain sufficiently high LWP in simulations with high ice concentration (more precipitation). Overall, the fluxes are small as expected and together with the subsidence they lead to stable clouds and especially ice concentrations.

Line 87-89: I don't understand why the existence of large rimed ice crystals are only indicative for the Hallett-Mossop and drop-shattering process. The efficiency of collisional break-up highly depends on ice particle size and riming (Phillips et al. 2017)

We removed this text because our new simulations show the effectiveness of the three SIP processes.

Line 243-245: RSx10 overestimates ICNCs and underestimates LWP. This is not addressed in the discussion. Overall it would be helpful if all ICNC and INP units are the same throughout the whole text to facilitate comparison. E.g. observations are given in L-1 , while all simulated values in kg-1.

ICNC is the only target value, but we will clarify that 1000 kg^{-1} is the concentration that should be reached to achieve the closure with observations. The upper limit in observed ICNC is much higher (10 000 kg^{-1}), and it is never reached in our simulations. At the cloud top where ice particles smaller than 200 μm can be included in the total concentration, the profile average ICNC values are close to 10 L^{-1} but the standard deviation is large ranging from detection limit (0.01 L^{-1}) up to 100 L^{-1} (Fig. 7 in Järvinen et al., 2023). The same figure shows that when particles larger than 200 μm are excluded (due to observed shattering in the Particle Habit Imaging and Polar Scattering (PHIPS) and The Small Ice Detector Mark 3 (SID-3) probes), the mean is about 1 L^{-1} with much smaller standard deviation. Based on these values, the best estimate for ICNC is between 1-10 L^{-1} (range from 0.1 to 100 L^{-1}). In the original manuscript, we took the lower limit (1 $L^{-1} \approx 1000$ kg^{-1}) as the target value, which needs to be reached. We will clarify this in the revised manuscript.

LWP is an input value (related to the initial temperature and moisture profiles) for the free-running simulations where ice formation and precipitation can reduce LWP. In addi-

tion, the development of LWP depends on surface fluxes and subsidence, and in this case subsidence was adjusted so that LWP is not increasing too much in simulations with low ice concentration (see the comment above). The precipitation rate depends on ICNC and the onset time for SIP reaching significant levels. Thus, simulations with low ice concentrations agree with the initial LWP while simulations with realistic ice concentrations will have a lower LWP. Therefore, comparison with the observed LWP would give a wrong impression that LWP is too low when ice concentration is realistic.

We cannot fully avoid using different units, because the observational values are given in L^{-1}, but most model inputs (e.g., INP concentration) and outputs are mass-based. Instead of converting all model outputs (and inputs) to L^{-1}, we converted the observed ice concentrations to kg^{-1}. After all, this is a modelling study and the bias due to unit conversion (air density) is negligible for observational values that have large uncertainty ranges.

Figure 2: It should also illustrate a timeseries of IWP to assess which simulation is more realistic compared to the measured values (4.1–9.5 g m-2). A shaded area in the individual panels that indicates the observed ICNC, LWP and IWP ranges would also be very useful for evaluation

The observed IWP is based on ice water contents (IWC), which depends on an assumed mass-dimension (m–d) relationship. One m–d formulation gave the numbers mentioned above, but another formulation gave IWCs lower by an order of magnitude (Järvinen et al., 2023). Thus simulated IWP range from 1 to 7 g m^{-2} is within the observational range including uncertainty. Because the observational uncertainty covers the range of predictions, it is not practical to add such wide shaded area to the figures. Comparison between LWP observations and model predictions is not meaningful for the reason mentioned above (LWP is a model input or initial value, not a target).

As mentioned above, we aim at reaching ICNC of about 1000 kg^{-1}, which corresponds to the lower limit of observations. The upper limit ($10\,000\,kg^{-1}$) is never reached, so basically all our simulations (RSx10) are within the observed range. We will add a line representing the target (minimum) value of 1000 kg^{-1} to Figs 2 and 3.

Line 245-246: I don't understand why the RSx5 simulation is not considered more realistic since it better reproduces the observed ICNCs. It also gives more realistic LWP values within the observed range (48–82 g m-2). Could the time-delay of ICNC enhancement in this simulation be due to the short spin-up time? (not enough to allow cloud dynamics to develop in time, which are critical for many microphysical processes?)

As explained above, we aim at reaching ICNC of about 1000 kg^{-1} and the LWP is model input rather than a target value. It is true that RSx5 is realistic (or any multiplier between 5 and 10), and we will clarify this in the revised manuscript. The RSx10 was selected to reduce the computational cost of the SALSA simulations.

One hour spin-up time is enough to allow the development of vertical mixing (the first increase in LWP). But we also did a simulation where longer (2 hours) spin up did not have significant effect on the ICNC trend. Basically, it just delayed the increase in ICNC by one hour.

Line 250-251: This statement is not clear; what is considered high and low INP value? 'Moderate' values also produce the desired ICNCs when combined with SIP

High INP concentration (without SIP) refers to the simulation with INP concentration set to the target [minimum] ICNC, and low means the other simulations where INP concentration is smaller than the ICNC. We will clarify this in the revised manuscript.

Line 253: Not clear. What do you mean by the term 'removal mechanism'? Do you refer to cloud condensate removal, ice mass or liquid mass removal? The different LWP values for example suggest different impact on liquid mass removal mechanisms.

SIP reduces when either cloud liquid or ice particles are removed. We reformulate this to 'cloud water and ice removal mechanisms such as precipitation'. Surely, ice-ice and ice-droplet collisions also change the amounts of cloud ice and liquid, but precipitation has more direct effect.

Line 255-257: I am not sure to which sensitivity simulation in this study do you refer to. In their RS experiment they showed that the simulated ICNCs where 10-20 times lower the observed – not necessarily that the ice production rate should be multiplied by 10 (which is the case with SI rate in Young et al). In their DM10_SIP experiment indeed they multiplied primary ice production (DeMott et al 2010) by a factor of ten, but this simulation accounted for many SIP mechanisms (not just RS). The relevant statement should be more accurate to avoid misinterpretation. Moreover, they showed that the combination of RS with another SIP mechanism was essential to reproduce the observed ICNCs. Maybe along these lines or during the last section it should be discussed that the RS multiplier could actually account for the missing contribution of another SIP mechanism

This line refers to this (Page 1312 in Sotiropoulou et al., 2020): "Our results indicate that the combination of both RS and BR is a possible explanation for the observed ICNCs; the newly generated fragments by RS further fuel the BR process, resulting in substantial ice enhancement through the latter, compared to when only one mechanism is active. Interestingly, when only RS is accounted for, the multiplication effect has to be increased by about a factor of 10–20 to obtain a good agreement with the observed ICNCs, i.e., the same factor as that used in Young et al. (2019)." It is not fully clear if they did a simulation where rime splintering was multiplied by those factors. It is true that they conclude that RS with another SIP mechanism was essential to reproduce the observed ICNCs. Our new simulations show that RS is the dominating mechanism, and RS (with or without the other SIP processes) is too weak when using the default model setup.

Figure 3: It would be very useful to see how timeseries of LWP also differs between the two microphysical schemes. Again the observed range of values should be marked in the Figure to facilitate evaluation

We will add LWP but the observed ranges are not included as explained above (LWP is an input).

Section 3.2: In my opinion the similarities between the two simulation set-ups is overemphasized, while there is hardly any discussion about the obviously statistically significant differences. ICNC is 35% larger (which is mentioned), however IWP is also twice as larger in SALSA. LWP might also reveal notable differences.

We surely expected that the two very different models will give different predictions, and the models do show statistically significant differences (e.g., 2000 vs 3000 kg^{-1} for ICNC). This is much less than could be expected for this kind of case where SIP increases ice concentrations by orders of magnitude. The difference is also much smaller than the

range of observational values (at least an order of magnitude for ICNC). Since ICNC is essentially determining IWP, which is mostly reduced from LWP, also the IWP and LWP values differ. We will clarify that the predictions are similar considering the model differences and the case where SIP increases ice concentration by orders of magnitude.

Line 283: I guess SIP rates are added to the ice crystal number tendency equation in the code. Why is it stated here that ICNCs are not directly related to SIP rate?

The Hallett-Mossop parameterization does not depend on ICNC directly, but the parameterization is almost directly dependent on riming rate (Eq. 1 in the manuscript), which depends on both ICNC and cloud droplets. That's why there is no point in including riming rates in this discussion.

Line 316-317: I would also argue that SB despite being simplified, it agrees more with observations (ICNC, IWP, etc)

We cannot say which one is better, because observational uncertainties are much larger than the difference in model predictions.

Figure 7: Timeseries of IWP would likely be useful too

We will add IWP to the figure.

381-382: I still do not understand why collisional break up is not considered a potential mechanism. Have you looked for fragmented ice particles in the probe images?

As mentioned above, we ran simulations that include collisional breakup (and droplet shattering), and it was found much less effective than rime splintering.

The majority of the ice particles in the probe images were classified as needles or columns, and these habits were consistently imaged as intact crystals. In contrast, particles assigned to the "other polycrystal" category exhibit more complex morphologies, and it cannot be excluded that some particles in this class may represent fragments rather than intact crystals. However, the class covered typically <20% of all crystals.

Lines 409-410: I don't understand why a better fit to the temperature measurements was not used for the LES intitialization. Clearly the authors preferred to adapt a warmer and more unstable profile.

We will clarify the profiles are not directly fitted but are adiabatic (neutral/well-mixed) profiles below cloud top. The profile was selected so that the simulated cloud top temperature matches with the observed minimum value, which is important for SIP. The warmest case was selected simply because it is the most interesting for SIP (warm but high ice concentration) while the cooler and humid profiles were left to sensitivity tests. Overall, these setups cover the observed cloud top temperature and LWP ranges.

Conclusions: results related to the different microphysics schemes are not discussed

As explained above, we will clarify that the results are different but less than expected.

Typos:

Line 320: water content (LWC)

Changed to liquid water path (LWP)

Line 359 : Hallett

Fixed

Referee #2

This paper addresses the origin of the high ice particle concentrations observed in an Arctic mixed-phase cloud during the ACLOUD campaign, which is a topic that still raises several open questions. The main results show that the rime splintering (RS) mechanism alone cannot explain the observed ice crystal number concentrations (ICNC). The authors demonstrate that either increasing the RS efficiency by a factor of ten or modifying the model setup and parameterizations of microphysics can lead to more realistic ICNC values.

Overall, this is a good quality study. The combined use of both bin and bulk microphysics approaches is quite rare and strengthen the conclusions of the study. It is also very interesting to see that modifying the parameterizations of microphysics have a such large effect on SIP efficiency.

I see two main issues with the present study. First I don't understand why other SIP mechanisms are not considered, given that were studied in one previous study: Calderón et al. (2025) (https://doi.org/10.5194/egusphere-2025-2730). Even if the temperature range studied here is not optimal for a high efficiency of collisional breakup or fragmentation of freezing drops (more active around –15°C), these processes could still influence the ICNC. Secondly, while the sensitivity experiment are valuable, their design and presentation could be improved for greater clarity.

Despite these points, the study is of high quality and offers valuable insights into SIP. I recommend that the authors address the following points to further strengthen the manuscript before publication.

Major comments:

Although significant uncertainties remain regarding SIP, artificially increasing the rime splintering (RS) efficiency in the model seems a bit artificial, as the literature does not support such strong RS. This point should be more clearly emphasized in the study.

We fully agree that the increase is artificial as already mentioned in the text. This is simply the easiest way to reach targeted ice number concentration, which in this case is reasonable ice concentration (1000 kg^{-1}) produced by SIP.

Collisional breakup the breakup process has been shown to be effective in Arctic mixed-phase clouds (e.g., Karalis et al., 2022: https://doi.org/10.1016/j.atmosres.2022.106302 and Sotiropoulou et al., 2021: https://doi.org/10.5194/acp-21-9741-2021). Therefore, it would also be valuable to test whether collisional breakup or DS could explain the observed ICNC without artificially boosting the RS rate. If I am correct, these SIP mechanisms can be activated in SALSA, as done in Calderón et al. (2025)?

Calderon et al. (2025) used different SALSA version, but we implemented their collisional breakup (IIBR) and droplet fragmentation (DS) parameterizations and repeated the simulations. As shown above (and explained in the revised manuscript), RS is three orders of magnitude more efficient compared with IIBR or DS. The studies by Karalis et al. (2022), Sotiropoulou et al. (2021) and Calderón et al. (2025) examine cooler and thicker clouds, where the conditions are more favourable for IIBR and DS.

As ice crystal concentration is typically expressed in L^{-1}, I recommend using this unit instead of kg^{-1} for consistency with the INP units and the literature.

Instead of converting all model outputs (and inputs such as INP concentrations) to L^{-1},

we converted the observed ice concentrations to kg^{-1}. After all, this is a modelling study and the bias due to unit conversion is negligible for observational values that have large uncertainty ranges.

Lines 69-70: Although no large drops were observed, it would be useful to check whether the model generates any. The presence of such drops could potentially trigger DS.

The model generates large (rain) droplets, but their concentration is negligible. For example, the highest rain drop number concentration in simulations shown in Fig. 3 is less than $2000\,kg^{-1}$. As mentioned above, we did simulations where DS and IIBR are included, but RS dominates.

Lines 73-79: The presence of millimeter sized ice particles suggest that collisional breakup might occur.

As mentioned above, we included collisional breakup, but it was found ineffective.

Lines 137-141: It is is good point to highlight and discuss that.

Now we mention excluding ice particles as an example in the conclusions.

Section 2.2.2: The HM process in SALSA and the number of bins used are not described, unlike for the SB scheme. Adding this information would improve clarity for readers.

We will clarify that the HM parameterization in SALSA is identical to that in SB (Eq. 1). SALSA bins were described in Sect. 2.3, but this information is now updated (the number of bins is given) and moved to Sect. 2.2.2.

Lines 238-239: This statement seems too strong. I would suggest saying that RS is insignificant, rather than SIP in general, since other SIP mechanisms were not considered.

Other SIP mechanisms are considered in the revised manuscript, but only with SALSA. These simulations show that rime splintering dominates. We have clarified the manuscript so that RS is now mentioned in relevant places.

Figure 2: In the factor 10 multiplier experiment, the LWP decreases to approximately 40 g m^{-2}, which is a bit lower than the observed values of 48–82 g m^{-2} mentioned in Line 65. The factor 5 experiment appears to be more consistent with the observed range.

As explained above for Referee #1, LWP is used as model input (initial value) and not as target value. LWP decreases in these free-running (nudging not used) simulations depending mainly on ice concentration so that the decrease is larger with higher ice concentration. We also agree that the factor of five experiment produces reasonable ice concentrations.

Lines 255-257: The Sotiropoulou et al. (2020) study also mention that "*Only the combination of both rime splintering (RS) and collisional break-up (BR) can explain the observed ICNCs, since both of these mechanisms are weak when activated alone.*" This suggests that combining RS with other processes could give realistic ICNCs, rather than artificially increasing RS.

Other processes were tested, but RS is the most effective while the others have negligible impact. The other processes are important for cases with, e.g., thicker clouds or cooler temperatures.

Lines 267-269: It is good to highlight the computational cost of the two microphysics schemes.

This is now highlighted in the conclusions.

Section 3.3: for both Fig 5 and 6:

- The comparison between the 100 kg^{-1} RS×10 line and the 1000 kg^{-1} RS×0 line makes it difficult to determine whether the variations are due to turning off RS or changing the INP number. Adding an intermediate 100 kg^{-1} RSx0 line would allow isolating the effect of RS deactivation without altering the INP number.
- Suggestion: showing only one time per profile could make the figure more readable, as these lines are similar and not central to the discussion.

Note that the intermediate (100 kg^{-1} RS×0) line would differ very much from the other lines as ICNC in this case is about 100 kg^{-1} while in the other cases it is 1000 kg^{-1}. Surely, an order of magnitude lower ice concentration would mean that at least the ice parameters differ.

One time per profile: does this mean removing either SB or SALSA profiles or removing something else like times that differ? Or using the same time for all? Different times are used because SIP simulations require different time (depends on INP concentration and microphysics) to increase ice concentration so that SIP takes control and the observed target ice concentration is reached. Comparison is fair when each profile is selected so that the target ice concentration is reached, i.e., different time for each profile.

Section 3.4: Examining the effect of the model parameters on SIP production is very interesting. Including a table in the appendix summarizing all the tests would help readers, or at least more clearly mentioning the experiment names in the text.

Note that Table A1 already summarizes the parameters used in sensitivity tests. We added a link to that table. We also added the experiment names to the text in bold font.

Fig 7: Presenting sensitivity results first with a fixed RS multiplier would help, as varying both RS and model parameters complicates comparisons. I suggest separating the experiments into (1) varying model parameters with RS fixed, and (2) varying the RS multiplier to clarify their effects.

That would mean showing many simulations where SIP is either ineffective or too effective. To keep the results for (2) readable, we would need one new figure for each test, so seven new figures in total, which is quite a lot. Current figure is a summary from such simulations showing only the relevant ones. Single figure is also better for comparing the relevant simulations.

Lines 340-342: Yes, this is an excellent point to highlight.

This is now highlighted in the conclusions.

Lines 343-349: This is very interesting. Why not test other temperature curves here as well?

The tested temperature curve represents a highly efficient one. Using a less efficient one would mean that the required RS multiplier is between 3 and 10. Since Fig. 7 is already quite full, adding more lines is probably not a good idea.

Conclusion: It might be important to mention that the RS multiplier is somewhat artificial and does not directly reflect observations of this process and is primarily used to achieve

the observed ice particle concentrations. This point is particularly relevant regarding the study of Seidel et al. (2024), which questions the RS efficiency.

We clarified that the multiplier is artificial.

Lines 393–394: Yes, other SIP processes may occur at colder temperatures, but it is important to keep in mind that collisional breakup can also happen between -3 and -8°C like RS or even between 0 and –3°C, unlike RS.

We tested the other SIP processes and explain the findings in the revised manuscript.

Minor comments:

Lines 87-90: The first sentence indicates that DS may occur, whereas the second one suggests it does not. I understand the message but this is a bit is confusing and could be clarified.

This text is now deleted as DS is included in the revised SALSA simulations.

Lines 196-200: could be moved to the previous section about SALSA microphysics.

Done.

Lines 383-386: The Lawson et al. (2015) parametrization has no temperature dependency, it is only parameterized as as function of drop size. But yes the DS process is fore sure dependent on temperature as showed for example recent experiments of Keinert et al. (2020). (https://doi.org/10.1175/JAS-D-20-0081.1)

We modified the discussion as DS (not based on Lawson et al., 2015) is actually tested and found irrelevant.

Lines 390-391: In my opinion, it is more due to the fact that no parametrization was available for DS until the paper of Lawson et al. (2015) and that the RS parametrization was used and available since decades.

We modified the discussion as DS (not based on Lawson et al., 2015) is actually tested and found irrelevant.

Changes made in the manuscript.

All changes made in the manuscript are shown below. New text is shown with the blue font color and deleted text with red font color. Figure 2 is new, so figure numbers have changed. Since simulations with SALSA microphysics were revised, all figures containing SALSA results have been updated, but the changes are minimal. Original Figs. 2 and 3 were updated based on referee comments. The document below includes both the original and the revised figures (and captions). The original figures are shown before (or above) the corresponding revised figures so that the caption of the original figure is replaced by text indicating the figure number in the previous manuscript version.

Can rime splintering explain the ice production in Arctic mixed-phase clouds?

Tomi Raatikainen[1], Silvia Calderón[2], Emma Järvinen[3], Marje Prank[1], and Sami Romakkaniemi[2]

[1]Climate System Research Unit, Finnish Meteorological Institute, Helsinki 00560, Finland
[2]Atmospheric Research Centre of Eastern Finland, Finnish Meteorological Institute, Kuopio 70211, Finland
[3]Institute for Atmospheric and Environmental Research, University of Wuppertal, Wuppertal, Germany

Correspondence: Tomi Raatikainen (tomi.raatikainen@fmi.fi)

Abstract. Secondary ice production (SIP) can increase ice crystal number concentration (ICNC) by several orders of magnitude, particularly in clean clouds with low concentrations of ice-nucleating particles (INPs). The most common SIP process in models is rime splintering (RS) also called as the Hallett-Mossop process. The generally adopted RS-formulation gives 350 splinters per milligram of rimed ice at the temperature of 268 K. We used large-eddy simulations to examine if rime splintering could explain the high ICNC observed during the ACLOUD (Arctic CLoud Observations Using airborne measurements during polar Day) campaign where cloud temperatures close to 268 K are favourable for rime splintering. With the default model setup, the splinter production rate had to be multiplied by a factor ten to close the gap between modelled and observed ICNCs. Similar changes have been made in other modelling studies. The factor of ten multiplier helped to trigger SIP so that it became a self-sustaining process, fully independent of the primary freezing initiated by INPs. Our simulations reached realistic steady-state ICNCs and maintained stable mixed-phase clouds through the 24-hour simulation time. Additional sensitivity tests showed that the efficiency of SIP depends strongly on model parametrizations and (e.g., fall velocity–mass–dimension parametrizations and those describing the dependency of SIP on temperature and particle size and habit) and air temperature, so that simulations with a modified setup were able to reproduce the observed ICNCs without the factor of ten multiplier.

1 Introduction

Shallow mixed-phase clouds (MPCs) are common over cooler high-latitude marine regions (Mioche et al., 2015; Listowski et al., 2019). Their important role in the formation of precipitation and the radiation budget make them highly sensitive elements in global climate and weather models (McFarquhar and Cober, 2004; Prenni et al., 2007; Cesana and Storelvmo, 2017; Korolev et al., 2017). Clouds reflect most of the incoming short-wave solar radiation, but they also cause long-wave warming, which can cause sea-ice melting over high-latitudes. This is one of the main drivers of the Arctic amplification (Previdi et al., 2021).

Global climate models struggle representing MPCs mainly because of low spatial and temporal resolutionand simplified cloud microphysics. MPC are inherently unstable thermodynamic systems, highly sensitive to turbulent surface fluxes and aerosol perturbations in the cloud condensation nuclei (CCN) and ice-nucleating particles (INP) number concentrations (Eirund et al., 2019; Gierens et al., 2020). Another challenge in modelling MPC comes from their susceptibility to experience secondary ice production (SIP), which can produce ice crystal number concentrations (ICNC) up to four orders of magnitude higher than

INP number concentrations Luke et al. (2021). Field campaigns such as the Mixed-Phase Arctic Cloud Experiment (M-PACE) (Zhao et al., 2021), the Ny-Ålesund AeroSol Cloud Experiment (NASCENT) (Pasquier et al., 2022) and the Aerosol-Cloud Coupling And Climate Interactions in the Arctic (ACCACIA) (Sotiropoulou et al., 2021) offer robust observational evidence of the occurrence of SIP in Arctic clouds, not only due to large differences between ICNC and INP number concentrations, but also due to the presence of fragments of frozen drops, needles and sheaths as well as broken dendrite branches in images obtained from in-cloud sampling systems (Rangno and Hobbs, 2001; Young et al., 2016; Pasquier et al., 2022).

The three most studied SIP processes relevant for mixed-phase clouds are: 1) rime splintering also known as the Hallett-Mossop process, 2) droplet shattering during freezing and 3) ice-ice collisional breakup. Fragile ice crystals like dendrites may break up mechanically when colliding with another large ice particle (Takahashi et al., 1995; Phillips et al., 2017). The process is effective at cooler most effective at temperatures around -15 °C. When the surface of a large drizzle droplet freezes, e.g. by contact with an ice particle, the resulting pressure increase within the droplet may cause the ice surface to break, which releases small ice fragments, or the droplet may eject an ice particle (Phillips et al., 2018; Keinert et al., 2020). Recent observations (e.g., Keinert et al., 2020) have shown that the process can take place at temperatures well above -10 °C but then the droplet needs to be large to produce significant number of secondary ice particles. The most studied SIP process is rime splintering (Hallett and Mossop, 1974) where fragile heavily rimed ice particles release ice splinters when colliding with large drizzle droplets, although the exact mechanism is not well known (Seidel et al., 2024). The process is most effective at temperatures close to -5 °C.

In this study we performed ten meter-resolution large-eddy simulations (LESs) using the University of California Los Angeles Large Eddy Simulation model combined with the two-moment cloud microphysics scheme of Seifert and Beheng (2006) (UCLALES-SB) and with the Sectional Aerosol module for Large Scale Applications cloud microphysics scheme (UCLALES-SALSA) to investigate the interplay between primary and secondary ice production processes, which can determine the phase and longevity of Arctic mixed-phase clouds. Our LES study is based on observations from the ACLOUD (Arctic CLoud Observations Using airborne measurements during polar Day) campaign carried out at north-west of Svalbard (Norway) in May-June 2017 (Ehrlich et al., 2019). Due to the observed conditions showing the absence of large drizzle drops and ice particles and cloud top temperatures close to -5 °C, we will focus on the rime splintering expected that rime splintering is the dominating SIP process. Our first aim is simulations confirmed this expectation, but these also showed that rime splintering is not strong enough to produce significant ice concentrations. First, we will examine if we can artificially increase rime splintering to examine what kind of adjustments (if any) are needed for the rime splintering parametrization to reproduce the observed ice concentration. Then we will examine the impacts of meteorological and modelling uncertainties on secondary ice production. We will also examine if the results are sensitive on microphysics by comparing two-moment and sectional representations. Overall, our study aims to quantify the potential of Hallett-Mossop process in representing secondary ice production in such warm mixed-phase clouds.

2 Methods

2.1 The ACLOUD campaign

Current LES simulations are based on observations from the Arctic CLoud Observations Using airborne measurements during polar Day (ACLOUD) campaign (Ehrlich et al., 2019). The campaign included airborne observations from the Arctic boundary layer and clouds to understand their roles in Arctic amplification. Low-level clouds were frequently observed during a warm and moist period from May 30 to June 12, 2017 (Wendisch et al., 2019). Here we focus on three flights with the Polar 6 aircraft conducted on the 2nd, 4th, and 5th of June when mixed-phase clouds were observed. These observations and the data analysis are described in detail by Järvinen et al. (2023), so a summary focused on the model simulations is given here. During the three flights, there was a uniform non-precipitating cloud deck above pack ice in a region North of Svalbard (the current focus region is 8.5–12.0 °E and 81.1–81.4 °N). Our simulations will be focused on the 2nd of June flight, which is the one with the highest observed ice crystal concentrations and cloud top temperatures, but we will use the two other flights to assess the impact of variability of meteorological conditions.

As reported by Järvinen et al. (2023), cloud liquid (LWP) and ice (IWP) water paths were in the range of 48–82 $\mathrm{g\,m^{-2}}$ and 4.1–9.5 $\mathrm{g\,m^{-2}}$, respectively, for the three flights. Cloud base heights were between 100 and 200 m while the cloud top height was consistently about 440 m. The maximum cloud droplet number concentrations (CDNCs) from average vertical profiles (Järvinen et al., 2023, Fig. 6) varied between 66 and 152 $\mathrm{cm^{-3}}$. These correlate with the above-cloud aerosol concentrations ranging from 125 to 173 $\mathrm{cm^{-3}}$. Measured droplet size distributions showed the absence of large drizzle droplets. Namely, the largest liquid droplets were about 30 $\mu\mathrm{m}$ in diameter (Supplementary material in Järvinen et al. (2023)). The observed cloud top temperatures ranged from -6.7 to -4.6 $^\circ\mathrm{C}$. Figure A1a shows the observed temperatures along with the idealized initial profiles for the model simulations (see Sect. 2.3).

Non-spherical ice particles in the diameter range from 9 to 1550 $\mu\mathrm{m}$ were detected using three different instruments as explained by Järvinen et al. (2023). Particle shattering due to collisions with the probes had an impact on concentrations at the lower part of the cloud, and if such shattering was observed then ice particles smaller than 200 $\mu\mathrm{m}$ were excluded. The maximum 10 s average ice crystal number concentrations at the upper part of the cloud varied between 10 and 18 $\mathrm{L^{-1}}$ (Järvinen et al., 2023) while the mean was close to 1 $\mathrm{L^{-1}}$ The maximum ice crystal number concentrations at the upper part of the cloud are about 10 $\mathrm{L^{-1}}$ while the concentrations for particles larger than 200 $\mu\mathrm{m}$ at the lower part of the cloud are about 1 $\mathrm{L^{-1}}$ (Järvinen et al., 2023, Fig. 7). The expected range of ice concentration is thus 1–10 $\mathrm{L^{-1}}$, which is in line with other observations from that region (e.g., Mioche et al., 2017). The ice particle shape observations showed that most particles were single crystals including needles and columns. In addition, significant fraction (38.5 %) of the observed ice crystals were rimed.

Ice-nucleating particles (INPs) are needed to initiate primary ice formation at the observed cloud temperatures (Kanji et al., 2017). There were no airborne INP measurements, but some ship-based measurements are available although only at -22.5 $^\circ\mathrm{C}$ temperature (Wendisch et al., 2019). Even at such a low temperature, measured daily (June 2–5, 2017) INP concentrations are in the order of 0.1 $\mathrm{L^{-1}}$. These measurements rule out possible pollution episodes and indicate that low INP concentrations can be expected for the region of interest. The best literature estimates for INP concentration at the cloud top temperature of about

-5 °C is in the order of 1×10^{-3} L^{-1} (e.g., Kanji et al., 2017; Murray et al., 2021; Li et al., 2022). This is significantly less than the observed cloud ice concentration of about 1 L^{-1} (Järvinen et al., 2023, Fig. 7). The three orders of magnitude difference between the INP and ice concentrations indicates that there is at least one active SIP process. The existence of large rimed ice crystals and the -5 °C cloud temperatures indicate that rime splintering (Hallett and Mossop, 1974) and droplet shattering during freezing (Phillips et al., 2018; Keinert et al., 2020) could be the dominating SIP mechanisms. However, droplet shattering is limited to large drizzle droplets which were not observed, so rime splintering is the most likely SIP process.

2.2 UCLALES-SALSA

UCLALES-SALSA (Tonttila et al., 2017; Ahola et al., 2020) is the LES model used in this study. SALSA refers to the sectional aerosol-cloud microphysics, which was added to UCLALES as an additional module. UCLALES (Stevens et al., 1999, 2005; Stevens and Seifert, 2008) with the default "SB" two-moment bulk microphysics by Seifert and Beheng (2001) is a commonly used LES model especially for liquid clouds (e.g., Ackerman et al., 2009; Seifert and Heus, 2013; van der Dussen et al., 2013). In this study we also use the more recently updated two-moment bulk ice microphysics (Seifert and Beheng, 2006; Seifert, 2008; Seifert et al., 2012, 2014; Blahak, 2008; Noppel et al., 2010), which is also used in large scale models (Seifert et al., 2012; Hohenegger et al., 2023). For clarity, this model version is referred to as UCLALES-SB. Both model versions share the same LES framework including radiative transfer and surface interactions and only their microphysics differ.

Computationally light but simplified SB microphysics allows conducting hundreds of simulations, which is useful for tasks like sensitivity tests where the impacts of model parameters on predictions is quantified. SALSA microphysics allows explicit modelling of aerosol-cloud-ice processes but this comes with a significant computational cost. By comparing predictions from both SB and SALSA microphysics, we can see the impact of the level of microphysical details.

2.2.1 SB microphysics

Liquid clouds in UCLALES-SB are diagnostic, which means that cloud water mixing ratio is diagnosed by using the saturation adjustment approach and a fixed cloud droplet number concentration is specified as a model input. The two-moment rain microphysics by Seifert and Beheng (2001) describe both total mass and number concentrations while size distribution is assumed to follow a fixed gamma-distribution. Rain drop formation is based on a autoconversion parametrization and then the droplets can grow by condensation of water vapour and by collecting cloud droplets and smaller rain drops. The liquid-cloud scheme was extended for mixed-phase and ice clouds by Seifert and Beheng (2006); Seifert (2008); Seifert et al. (2012, 2014). The solid particle types include ice, snow, graupel, and hail, which have both mass and number as prognostic variables. The two-moment scheme accounts for various interactions between liquid and solid particles. The details are given in the original publications, so only a brief description is given here. The ice category represents small ice crystals formed by ice nucleation that are growing mainly by deposition of water vapour. In the absence of prognostic aerosols and thus INPs, primary ice nucleation is parametrized, so that the in-cloud ice crystal number concentration depends only on temperature. Collisions of ice with cloud droplets and larger rain drops leads to rimed ice, and depending on the resulting particle size, those particles are

described by the snow, graupel and hail categories. Further riming and accretion lead to even larger particles and the resulting type is determined based on the size and type of colliding particles.

In this study we use hydrometeor parametrizations (fall velocity–mass–dimension parametrizations, parameters of the gamma-distribution, and mass limits) from Seifert et al. (2012) with the exception that fall velocity–mass–dimension parametrization for ice which is from Seifert et al. (2014). This change was made because the mass–dimension parametrization of ice from Seifert et al. (2012) produces exceptionally high dimensions compared with those from any other parametrization used in our simulations. Järvinen et al. (2023) used mass–dimension parametrizations from Brown and Francis (1995) to calculate the ice water path (IWP) from the measured particle size. This parametrization, which happens to be the same as the Seifert and Beheng (2006) snow parametrization, gives the same mass for 1.2 mm particles as the parametrization by Seifert et al. (2014). For particles smaller than 1.2 mm, the Brown and Francis (1995) parametrization gives higher mass than the parametrization by Seifert et al. (2014). Because simulated particles are typically smaller than 1.2 mm, the Brown and Francis (1995) parametrization gives smaller dimension than that from Seifert et al. (2014). This will be examined in Sect. 3.4.

The only SIP process included is rime splintering (Eq. 1). Splinter production rates (dN_i/dt, s^{-1}) are parametrized as product of constant $350\,\mathrm{mg}^{-1}$ giving the number of splinters per milligram of rime, temperature-dependent efficiency term $f(T)$, and water mass riming rate dm_{rime}/dt ($\mathrm{kg\,s}^{-1}$) (e.g. Hallett and Mossop, 1974; Cotton et al., 1986; Reisner et al., 1998). The efficiency is linear between the minimum (zero at 265 K), optimal (one at 268 K) and the maximum (zero at 270 K) temperatures. We assume that splinters are small and therefore assign them to the ice category.

$$dN_i/dt = 350\,\mathrm{mg}^{-1}\, f(T) dm_{\mathrm{rime}}/dt \tag{1}$$

This parametrization includes rime mass (dm_{rime}/dt) from collisions between any liquid droplet and solid ice particle. Notably, any limits for droplet diameter such as 25 µm minimum (e.g., Ferrier, 1994; Sullivan et al., 2018a) are excluded as it would require calculating incomplete gamma functions. Also, the size limits are more important for parametrizations where the number of splinters depends on the number of droplets collected (Field et al., 2017). Some studies have also limitations for particle types that can produce splinters, for example, Kudzotsa et al. (2016), Sullivan et al. (2017, 2018b), and Sotiropoulou et al. (2021) exclude ice particles while Sullivan et al. (2018a) include those. In this case, ice happens to be the dominant frozen particle type, so excluding it would essentially prevent secondary ice productionrime splintering.

UCLALES-SB has mass concentration and the average maximum dimension thresholds for all collisions including riming, which have no physical meaning but presumably were used to reduce computational costs. For example, the default minimum total ice water mixing ratio and dimension are $10^{-5}\,\mathrm{kg\,m}^{-3}$ and 150 µm, respectively, for ice-cloud collisions (the corresponding limits for cloud are $10^{-6}\,\mathrm{kg\,m}^{-3}$ and 10 µm). A dimension of 150 µm is not a real limitation for the currently used mass–dimension parametrization of ice. However, $10^{-5}\,\mathrm{kg\,m}^{-3}$ is a high value considering the low primary ice concentration and the slow depositional growth rates. Thus, for all simulations here, we set the solid particle concentration limits to $10^{-9}\,\mathrm{kg\,m}^{-3}$, which is the same as the threshold concentration for rain. Atlas et al. (2020) made the same conclusion on concentration limits when simulating cumulus clouds over the Southern Ocean. Likewise, Schäfer et al. (2024) reduced thresholds so that rime splintering could happen in their simulations with Morrison et al. (2009) microphysics based on the Ny-Ålesund

Aerosol Cloud Experiment (NASCENT). Similar adjustments have been made by Huang et al. (2008), Young et al. (2019), and Sotiropoulou et al. (2021).

2.2.2 SALSA microphysics

Cloud microphysics in UCLALES-SALSA is treated using a sectional (bin) approach where aerosol, cloud, rain, and ice are described using several size sections (bins) for which microphysical processes are calculated. The liquid and ice cloud microphysics are originally described by Tonttila et al. (2017) and Ahola et al. (2020), respectively. The bins keep track of chemical composition (mass of solutes and water) and the number of aerosol particles and hydrometeors. Aerosol and cloud droplet size bins are based on the dry particle size, which includes solutes but not water and assumes a spherical particle shape. Rain droplet size bins are based on the wet size that accounts for the droplet volume including solutes and water. For ice we also use liquid water-equivalent wet size bins which are independent of the assumed ice particle shape. The wet size is basically the same as the size of a liquid droplet resulting in from ice being melted. Here, the aerosol is described with 12 logarithmically distributed dry size bins from 10 nm to 3 $\mu\mathrm{m}$. Cloud bins are based on aerosol bins, but they do not include the first three bins (nucleation mode) as these particles are too small to activate. Seven logarithmically distributed rain bins range from 50 to 2000 $\mu\mathrm{m}$ and ten ice bins from 10 to 2000 $\mu\mathrm{m}$ (water-equivalent wet diameter).

Water is allowed to partition between vapour, liquid and ice phases based on equilibrium conditions at the droplet (so-called κ-Köhler; Petters and Kreidenweis (2007)) and ice particle surfaces. Water vapour flux is diffusion-limited and related to ambient saturation ratio, thus this non-equilibrium approach allows the prediction of supersaturation and cloud activation without any additional parametrizations. Here cloud activation means that when the wet size of an aerosol bin exceeds the critical droplet size, it is moved (partially or completely) to a corresponding cloud bin. Rain drop formation can be based on either autoconversion-like bulk parametrization from SB microphysics (e.g., Seifert and Beheng, 2001) or counting the cloud-cloud collision where the resulting droplet size exceeds a threshold often set to 20 microns (Tonttila et al., 2021). Independent of the origin, rain drops will grow mainly by colliding with smaller cloud and rain droplets and eventually precipitate if conditions are suitable. Because liquid precipitation was not observed and simulated rain water paths were negligible, we will use the simple autoconversion-like bulk parametrization.

For this study, we implemented the same rime splintering parametrization as used in the SB microphysics (Eq. 1). SALSA microphysics has certain concentration limits for all processes including riming, but the limits represent numerical accuracy of the model. Additional size limits are available for calculating the riming rate for the rime splintering process. The limit was set to 10 $\mu\mathrm{m}$ for cloud droplets, rain drops and ice particles. This means that the smallest cloud droplet bins can be excluded while all rain drops and ice particles are typically larger than 10 $\mu\mathrm{m}$. When the size and particle type limits for riming and rime splintering are essentially removed, both SALSA and SB microphysics have similar chances to produce secondary ice particles.

In addition to the rime splintering, we implemented the Phillips et al. (2018) and Grzegorczyk et al. (2025) parametrizations for droplet shattering (DS) and ice-ice collisional breakup (IIBR), respectively. The latter is based on parametrization developed byPhillips et al. (2017) but has revised parameters. Previously, Calderón et al. (2025) implemented these pro-

cesses into another SALSA version, so here we implement these into our SALSA version. Some IIBR parameters depend on rime mass fraction, but this is not predicted in our SALSA version. Therefore, we use parameters for unrimed particles, which have rime mass fraction less than 0.5. Grzegorczyk et al. (2025) parametrization expects that only those collisions where ice crystals are not sticking together can produce secondary ice. We set the ice-ice sticking efficiency to 0.2, which is similar to the rime mass fraction dependent values used by Grzegorczyk et al. (2025) and Calderón et al. (2025). Here DS includes both cloud and rain droplets, just as rime splintering. The parametrization for Mode 1 (small ice, large drop) droplet shattering is limited to droplet diameters larger than 50 µm and temperatures below 270.15 K while Mode 2 (large ice, small drop) is limited to droplet diameters larger than 150 µm (Phillips et al., 2018). Size or temperature limits are not applied to IIBR.

2.3 LES setup

Adjustable model parameters are given in Table A1. The LES domain covers a horizontal area of $10\,\mathrm{km} \times 10\,\mathrm{km}$ and extends vertically up to $1\,\mathrm{km}$. Horizontal resolution is $100\,\mathrm{m}$ and vertical resolution is $10\,\mathrm{m}$ below $600\,\mathrm{m}$. Above $600\,\mathrm{m}$, vertical resolution increases by 3 % for each vertical level. Simulations have a maximum time step of $1\,\mathrm{s}$ and the total simulation time is 24 hours where the first hour is with liquid clouds only (spin-up). The spin-up is used to allow the development of turbulence in a liquid cloud before particle sedimentation and rain and ice microphysics are fully included. For short-wave radiation, the solar zenith angle is fixed to 60° to match with the observations made during 1–2 hours around the local noon in early June. In addition, following Järvinen et al. (2023), sea surface albedo is set to 0.5, which represents partial ice cover over pack ice. Long-wave emissions are based on the surface temperature, which is set to be the same as that of the initial atmospheric profile at the lowest model level. For pack ice we set the surface roughness to $0.04\,\mathrm{m}$ (see, e.g., Weiss et al., 2011). Latent and sensible heat fluxes are set to 15 and $0\,\mathrm{W\,m^{-2}}$, respectively, based on initial tests where the fluxes were simulated. Large scale subsidence is described with a constant divergence of $5\times10^{-6}\,\mathrm{s^{-1}}$. This relatively large value was selected to limit the increase in cloud top height and LWP driven by radiative cooling.

Statistics are calculated every 2 minutes, and this is the output frequency of domain mean statistics. Horizontally and time-averaged profiles, and vertically integrated instantaneous column outputs are saved every 10 minutes.

For SB microphysics, we set the base case CDNC to $80\times10^6\,\mathrm{kg^{-1}} \approx 100\times10^6\,\mathrm{m^{-3}}$, which is in the range of the observed maximum values from 66×10^6 to $152\times10^6\,\mathrm{m^{-3}}$ (Järvinen et al., 2023). For SALSA we assume ammonium sulfate aerosol (hygroscopicity parameter κ=0.6) so that the shape of the initial unimodal log-normal size distribution (D_g=106 nm and σ=1.81) is based on observations (see Fig. A2b) and the total aerosol concentration is set to $150\times10^6\,\mathrm{kg^{-1}}$. With this initial aerosol, simulated CDNC will be similar with the fixed value of $80\times10^6\,\mathrm{kg^{-1}}$ used by the SB microphysics. Aerosol is described with 12 logarithmically distributed dry size bins from 10 nm to 3 µm. Cloud bins are based on aerosol bins, but they do not include the first three bins (nucleation mode) as these particles are too small to activate. Rain bins range from 50 to 2000 µm and ice bins from 10 to 2000 µm (water-equivalent wet diameter). For SALSA ice, we use the same fall velocity–mass–dimension parametrizations from Seifert et al. (2014) as with UCLALES-SB.

Because we are focusing on SIP, we use a simple primary ice formation approach where the in-cloud INP concentration is given as an input value. In practice, this means that cloud droplets freeze until the total ice concentration reaches the given INP concentration. As explained in Sect. 2.1, the expected INP concentration can be as low as $10^{-3}\,\mathrm{L}^{-1}$ or about $1\,\mathrm{kg}^{-1}$ (based on literature) but should not be larger than $0.1\,\mathrm{L}^{-1}$ or about $100\,\mathrm{kg}^{-1}$ (observed at -22.5 °C). So, with these LES simulations, we will test different INP concentrations including 1, 10 and $100\,\mathrm{kg}^{-1}$. These INP concentrations are from one to three orders of magnitude lower than the observed ice concentration of about at least $1\,\mathrm{L}^{-1}$ or about $1000\,\mathrm{kg}^{-1}$ (Järvinen et al., 2023). We will take this as our minimum target value, thus in all following simulations we aim to reach ice concentration of $1000\,\mathrm{kg}^{-1}$. We will also conduct a simulation where INP concentrations is set to $1000\,\mathrm{kg}^{-1}$ and SIP is switched off. This represents a modelling approach where high the observed ice concentrations can be reached even without SIP by using unrealistically high INP concentrations.

The initial temperature and humidity profiles were reconstructed based on the observed cloud extent, LWP, and cloud top temperature while also noting that these can change during the simulations. For example, ice formation and precipitation decrease LWP. The default profiles have specified surface temperature, relative humidity (RH) and pressure set to 1027 hPa, which allow the calculation of liquid water potential temperature (θ_L) and total water mixing ratio (r_t) at the surface. These are assumed to be constant throughout a well-mixed boundary layer. A linear water vapour mixing ratio and potential temperature jumps (-0.9 $\mathrm{g\,kg}^{-1}$ and 8 K, respectively) are assumed for the inversion layer (from 380 to 470 m), and above that the change is based on fixed gradients of -0.001 $\mathrm{g\,kg}^{-1}\,\mathrm{m}^{-1}$ for r_t and 0.01 $\mathrm{K\,m}^{-1}$ for θ_L. Figure A1a shows the observations along with the absolute temperatures calculated from these profiles (based on the saturation adjustment method). Additionally, Fig. A1b shows the observed and average wind components, which are used in all LES simulations.

The two additional initial profiles (cool and moist) were generated to test the impact of observational variability of the meteorological parameters. The cool profiles were generated by decreasing θ_L by 2 K and by decreasing r_t so that LWP is not changing. The moist profiles were generated by increasing r_t by $0.08\,\mathrm{g\,kg}^{-1}$. In this case, the latent heating within the cloud layer increases the absolute temperature compared with that of the default profile. Figure 1 shows the initial temperature and moisture profiles as well as absolute temperature and RH based on the saturation adjustment method.

3 Results

The first test simulations with UCLALES-SALSA showed that the SIP processes were not able to produce significant amounts of ice even with the highest INP concentration of $100\,\mathrm{kg}^{-1}$. Panel (a) in Fig. 2 shows the domain mean ice crystal number concentration (ICNC) for grid cells containing ice from two simulations: one without SIP and one with the three SIP processes switched on. Clearly, the ice concentrations are practically identical. Panel (b) shows the primary freezing rates and contributions from each SIP process (when SIP is on). Rime splintering (RS) produces about an order of magnitude less ice than primary freezing, but RS is still at least three orders of magnitude more efficient than ice-ice collisional breakup (IIBR) and droplet shattering (DS). Thus, in the following simulations we will focus on RS, but leave the other SIP processes on in all SALSA simulations. SB microphysics includes just rime splintering, and it is equally

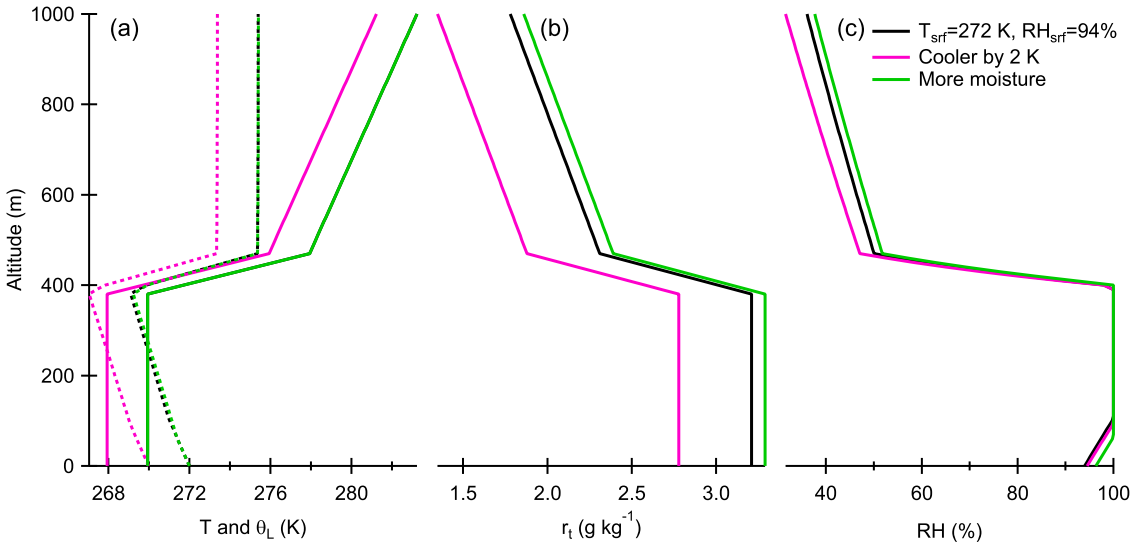

Figure 1. Initial (a) liquid water potential temperature (θ_L, K, solid lines) and (b) total water mixing ratio (r_t, g kg^{-1}) profiles for the LES simulations including the base case and the cool and moist cases. Panel (a) shows also the absolute temperature (T, K, dashed lines) and panel (c) shows RH (%), which were calculated from θ_L and r_t by using the saturation adjustment method.

inefficient in the corresponding simulations. Next we will use the computationally fast UCLALES-SB for exploring suitable adjustments for RS SIP.

3.1 Base case

The first test simulations with UCLALES-SB showed that SIP was inefficient even after releasing the constraints related to droplet size, mass concentration or type of hydrometeors involved in the formation of rimed ice. Young et al. (2019) showed that in addition to removing size and concentration limits, secondary ice production rime splintering had to be artificially increased to have an impact on ice concentration. So, to match with the observed exceed the observed minimum ice crystal number concentration of about 1000 kg^{-1}, we will first artificially increase secondary ice production was increased simply by multiplying rime splintering rate (Eq. 1) by a constant factor while the temperature-dependent efficiency term was retained. The impacts of other possible adjustment will be examined in Sect. 3.4 by means of sensitivity tests. Figure 3 shows UCLALES-SB simulations with different INP concentrations (1, 10, 100, and 1000 kg^{-1}) when rime splintering (RS) rates are multiplied by a constant factor (0, 1, 5, and 10). Panel (a) shows the domain mean ice crystal number concentration (ICNC) for grid cells containing ice and panel panels (b) shows and (c) show the horizontally averaged liquid water path ice (IWP) and liquid (LWP) water paths, respectively. It should be noted that the SB microphysics includes ice, snow, graupel and hail categories, but only ice is shown here and in the following figures. This is because ice concentration is typically about two orders of magnitude higher than the concentration of any other solid particle type.

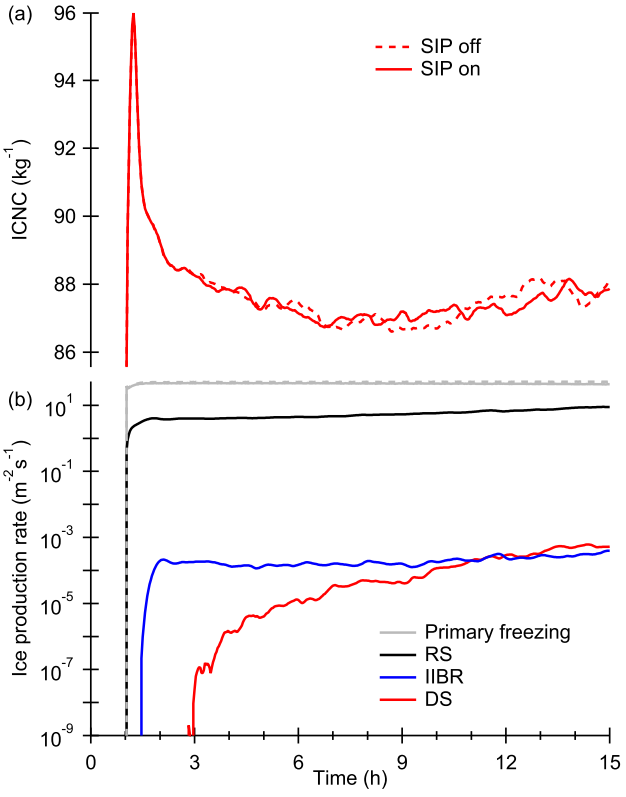

Figure 2. Simulated (a) domain mean ice crystal number concentration (ICNC) and (b) primary and secondary ice production rates for two SALSA simulations with INP concentration 100 kg^{-1} and SIP switched on (solid lines) and off (dashed lines).

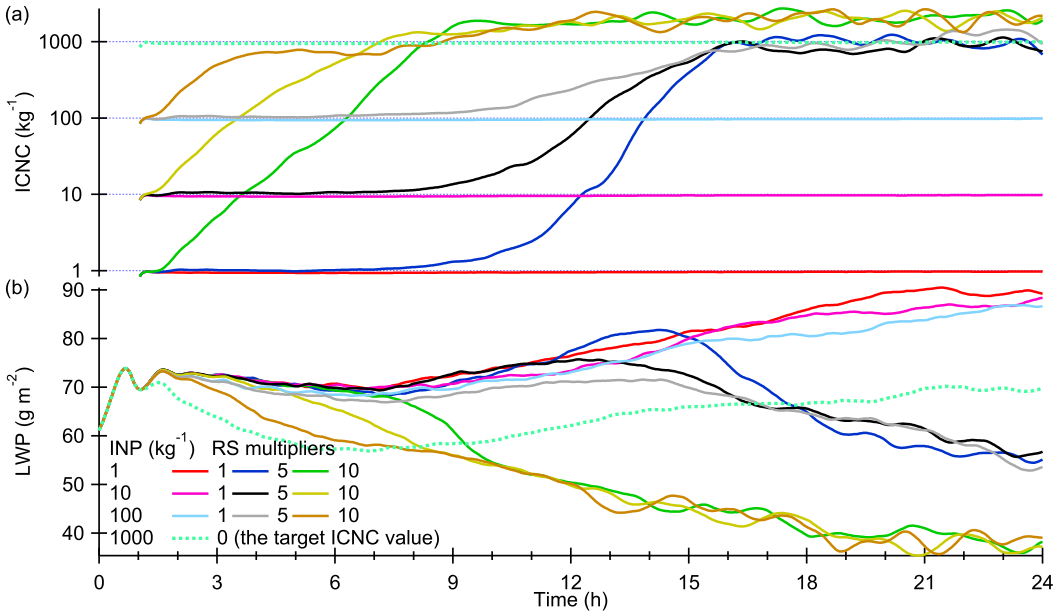

Original Fig. 2.

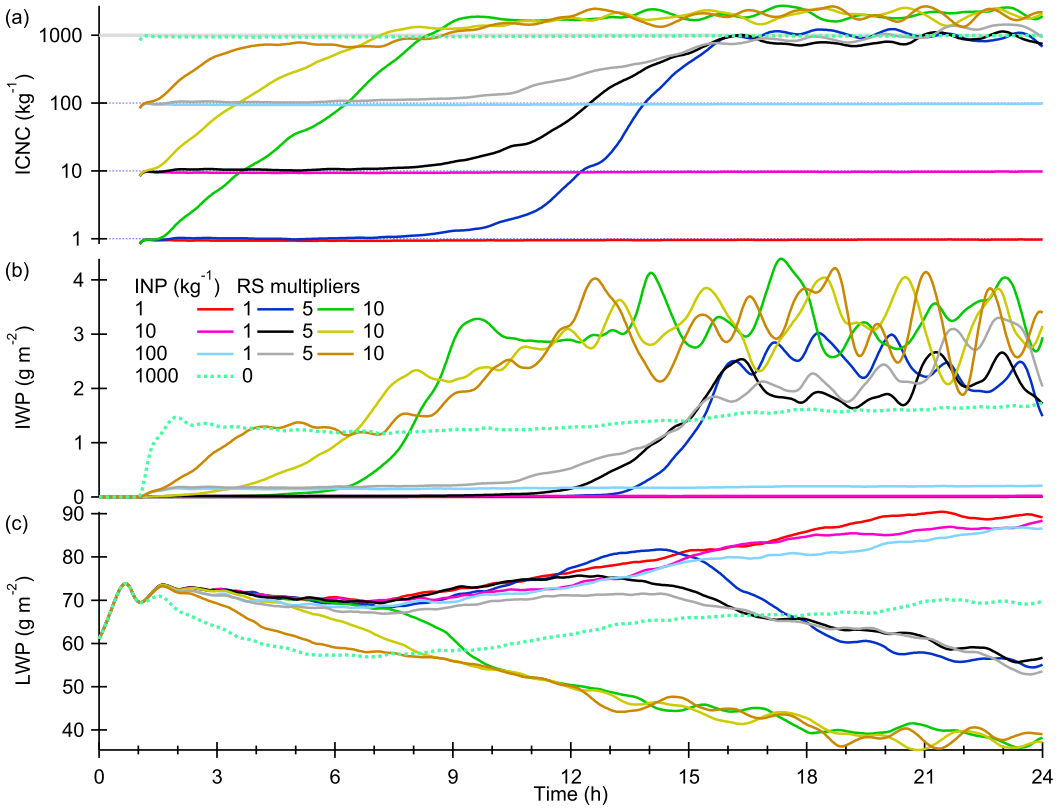

Figure 3. Simulated (a) ice crystal number concentration (ICNC)and , (b) ice water path (IWP) and (c) liquid water path (LWP) for the cases with different INP concentrations (1, 10, 100, and 1000 kg^{-1}) and multipliers for the rime splintering (RS) secondary ice production rate (0, 1, 5, and 10) from UCLALES-SB. The thick gray line shows the target ICNC of 1000 kg^{-1}.

The target (observed) ICNC of $1000\,\mathrm{kg}^{-1}$ is reached when INP concentration is set to that value and rime splintering is switched off by setting the multiplier to zero (the one dashed line). Simulations with more realistic INP concentrations of 1, 10 and $100\,\mathrm{kg}^{-1}$ and RS switched on (the unit multipliers) produce ice concentrations that are practically the same as the INP concentration, which means that RS secondary ice production is insignificant. Increasing the secondary ice production RS by a factor 5 does help, but it requires about 15 hours until the target ice concentration is reached. This is a long time compared to, for example, diurnal temperature variations which could trigger or prevent secondary ice production. Increasing the rate by a factor 10 means that SIP starts almost immediately after the spin-up and the target ice concentration is reached within 9 hours. Interestingly, the factor of ten increase is enough for INP concentrations ranging from 1 to $100\,\mathrm{kg}^{-1}$ to reach the same steady-state ice concentration of about $2000\,\mathrm{kg}^{-1}$. Basically, this means that a strong enough SIP becomes self-sustaining, so it no longer needs or depends on the primary ice formation. The same behaviour is seen in the simulations with a factor of 5 increase, but there is a significant time delay and the steady-state ice concentration is lower (about $1000\,\mathrm{kg}^{-1}$). Clearly, the more efficient SIP is able to maintain a higher steady-state ICNC and IWP, which is closely related to ICNC.

When ice concentration is in the order of $1000\,\mathrm{kg}^{-1}$ (with or without SIP), the cloud starts to precipitate ice, and the continuous ice production and removal causes the decrease in LWP. This decrease in liquid cloud water reduces SIP but has no direct impact on the INP concentration. Thus, cloud properties are different depending on how ice formation is modelled: with high INP concentration ($\approx$ICNC) without SIP or low INP concentration ($\ll$ICNC) and SIP producing most ice particles. Naturally, SIP accounts for the feedback between ice production and precipitation as well as any other removal mechanisms cloud water and ice removal mechanisms such as precipitation.

From now on, the factor of 10 increase in secondary ice production is considered as the base case setting for SB microphysics. Interestingly, to match with the observed ice concentrations, Young et al. (2019) needed to apply the same factor of ten adjustment to their rime splintering parametrization. Sotiropoulou et al. (2020) noted that when only the rime splintering process is accounted for, ice production had to be increased by about a factor of 10–20 to obtain a good agreement with the observed ice concentrations.

3.2 Comparison of cloud microphysical schemes

Figure 4 shows additional domain mean statistics from the four UCLALES-SB simulations (solid lines) described above and from the corresponding UCLALES-SALSA simulations (dashed lines). The reference simulations have INP concentration set to $1000\,\mathrm{kg}^{-1}$ and SIP is switched off (RS$\times$0). The three SIP simulations with INP concentrations set to 1, 10 and $100\,\mathrm{kg}^{-1}$ have the rime splintering (RS) ice production rate multiplied by ten (RS$\times$10). Time in this figure and in all SALSA simulations is limited to 15 hours, because this is enough for both SB (see Fig. 3) and SALSA simulations to reach a steady-state.

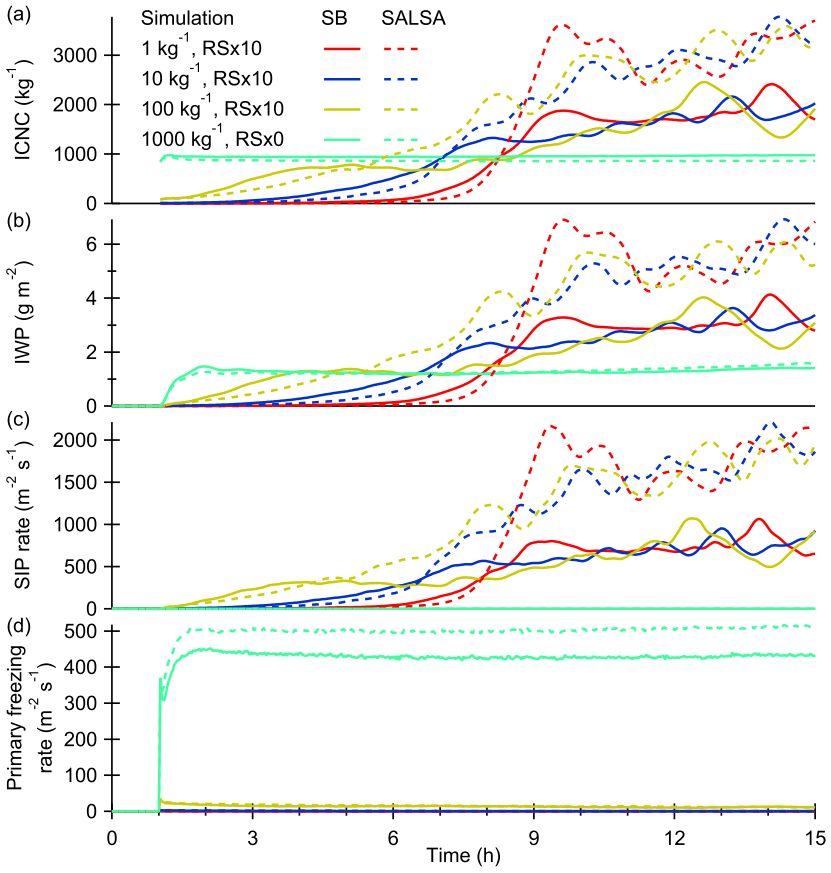

Original Fig. 3.

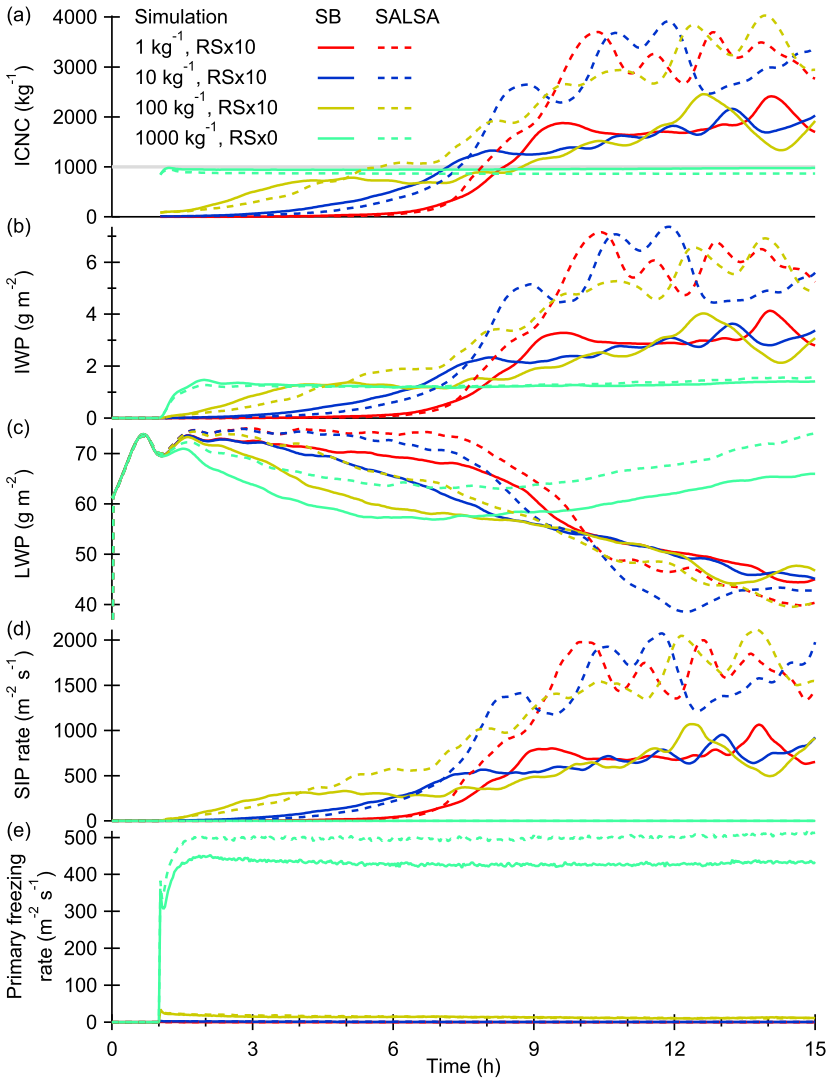

Figure 4. Simulated (a) ice crystal number concentration (ICNC), (b) ice water path (IWP), (c) liquid water path (LWP), (d) RS secondary ice production rate, and (de) primary cloud droplet freezing rate for the cases with different INP concentrations (1, 10, 100, and 1000 kg^{-1}) and multipliers for the rime splintering (RS) secondary ice production rate (0 or 10). The thick gray line shows the target ICNC of 1000 kg^{-1}.

The first thing that Fig. 4 shows is that initially SB has higher SIP rates and ice concentrations, but SALSA has higher steady-state SIP rates so that the final ICNC is about $3000\,\mathrm{kg}^{-1}$ while this for SB this is $2000\,\mathrm{kg}^{-1}$. Overall, however, SB and SALSA predictions are qualitatively similar , which is not always seen when comparing microphysical models that differ so much in complexity similar when considering the differences in complexity between the microphysical models and the case where SIP increases ice concentrations by orders of magnitude. In this case, the complexity influences the time needed to run a 24 h simulation: about 1 h 20 min with the two-moment SB and 29 hours with the sectional SALSA (parallel run with 100 CPU cores), i.e., there is a factor of 20 difference in computational costs. Clearly, the efficiency of SB makes it useful for conducting large numbers of test simulations while SALSA can provide additional details about the process.

Another thing that Fig. 4 confirms is that RS SIP rate (panel (cd)) exceeds the primary ice production rate (panel (de)) within two to eight hours depending on the INP concentration. When ice concentration becomes large enough (about $1000\,\mathrm{kg}^{-1}$), contribution from primary freezing becomes negligible. Thus, SIP maintains a feedback loop where INPs are not needed any more. This was confirmed by a test simulation, where switching off the primary freezing after 6 h had negligible impact.

The third thing that Fig. 4 reveals is that the SIP rate correlates linearly with ice crystal number concentration and ice water path (IWP). Indeed, calculating spatial and temporal correlations between SIP rate and various model outputs reveals that the highest absolute Pearson's correlation coefficients are seen for ice number concentration, water vapour deposition rate, and IWP. Table 1 shows Pearson's correlation coefficients for these variables (and LWP as a reference) calculated for both SB and SALSA simulations where the INP concentration is set to $100\,\mathrm{kg}^{-1}$ and SIP rate is multiplied by a factor of 10. Temporal correlation is calculated for the domain mean time series outputs and spatial correlation is calculated for snapshots of column-averaged or integrated 2D model outputs taken from the 7^{th} hour. These three independent, i.e., not directly related to the SIP rate like riming rate, variables clearly stand out. ICNC, water vapour deposition rate, and IWP represent the 1^{st}, 2^{nd} and 3^{rd} moment of the ice size distribution, respectively. The most obvious explanation is that SIP requires cloud droplet–ice collisions. Because cloud droplets and LWP are more evenly distributed, ice crystals are more important for the spatial correlation. The negative temporal correlation between SIP rate and LWP is related to the fact that ice is produced at the expense of liquid water, which is also apparent from Fig. 3. Luke et al. (2021) found a positive spatial correlation between observed vertical air velocity and SIP rates, but this is not that clear in our simulations, because the correlation coefficients (0.36 for SB and 0.25 for SALSA) are smaller than those for LWP. In fact, it looks like higher vertical velocities mean higher LWPs, which support ice production.

As an example, Fig. 5a shows the temporal correlation between domain mean SIP rate and IWP for all SB and SALSA simulations where RS SIP is enabled. Figure 5b shows a snapshot of vertically integrated SIP rate contours over IWP colourmap (SB simulation, INP=$100\,\mathrm{kg}^{-1}$, RS$\times$10, time=7 h). Clearly, the SIP rate contours match with the regions with high IWP.

Table 1. Spatial and temporal correlation between SIP rate and the three independent variables with the highest Pearson's correlation coefficients (Deposition rate, IWP, and ICNC) and additionally also LWP. Spatial correlations are calculated for the column-averaged model outputs taken from hour 7 while temporal correlation is calculated for the domain mean output time series. All simulations have INP concentration set to $100\,\mathrm{kg}^{-1}$ and SIP rate multiplied by a factor of 10.

	Spatial		Temporal	
Variable	SB	SALSA	SB	SALSA
LWP	0.60	0.55 0.50	-0.77	-0.93 -0.96
ICNC	0.82	0.92 0.91	0.91	0.97 0.99
IWP	0.90	0.94 0.93	0.90	0.95 0.99
Deposition rate	0.93	0.97 0.96	0.92	0.96 0.99

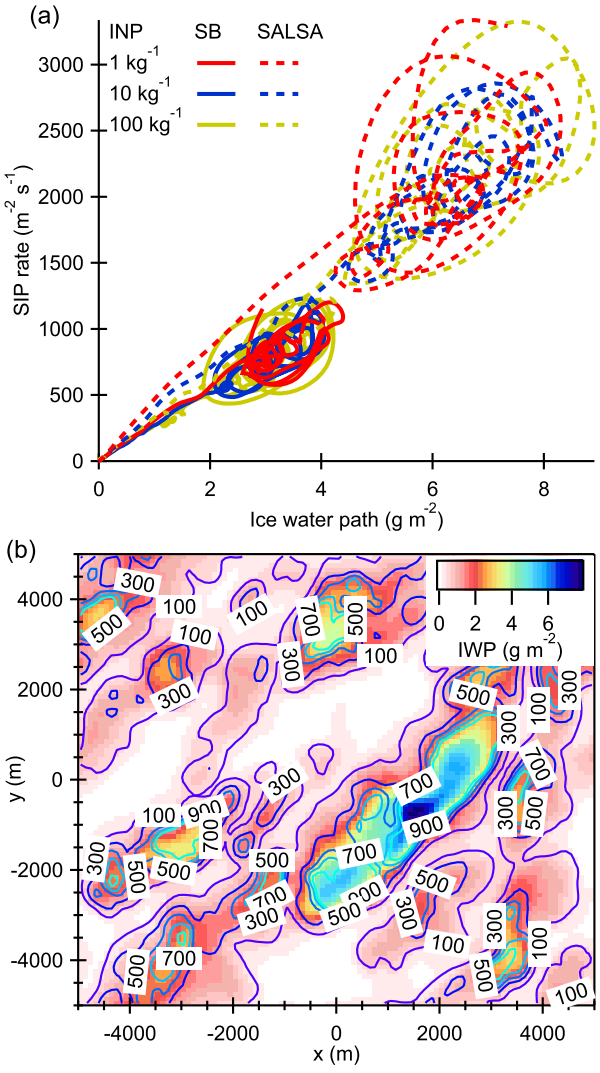

Original Fig. 4.

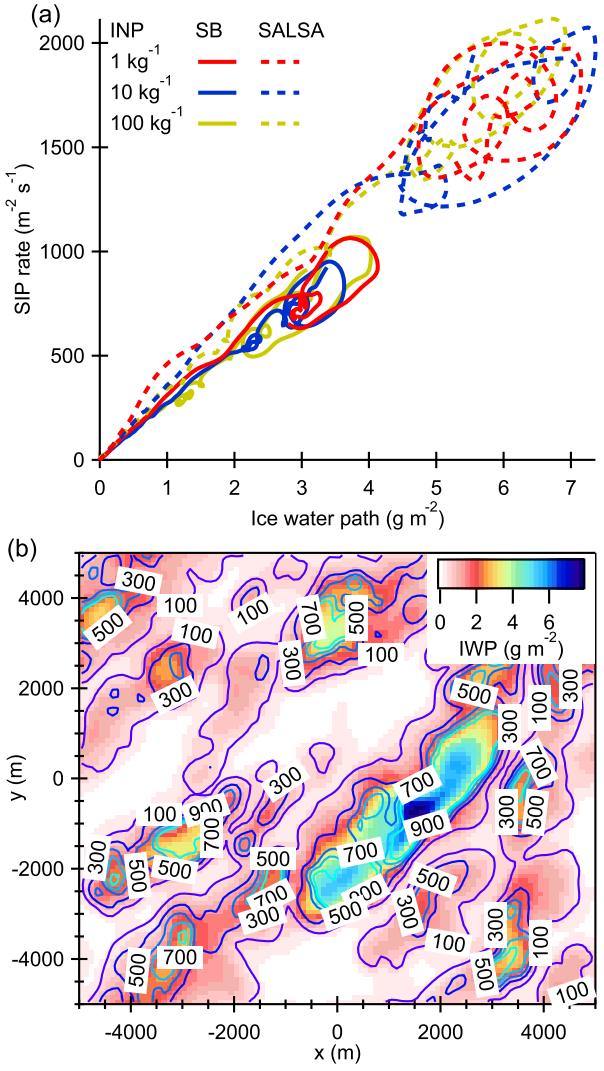

Figure 5. Simulated (a) domain mean RS SIP rate as a function of IWP for the six simulations from the first 15 simulation hours and (b) instantaneous (t=7 h) SIP rate contours (the change in column ICNC due to SIP, $\mathrm{m^{-2}\,s^{-1}}$) and IWP colourmap for the SB simulations with INP=100 $\mathrm{kg^{-1}}$ and SIP rate multiplied by a factor of 10.

3.3 Vertical distributions

Comparing Because the time to reach the target ice concentration of 1000 kg^{-1} depends on simulation (see Fig. 4), the horizontally averaged profiles of the cloud parameters (Fig. 6) shows fairly small differences especially when each profile is selected so that the are selected from the time step when ICNC reaches 1000 kg^{-1} for the first time (here we take the concentration at the altitude of 355 m). Therefore, it is not surprising that the profiles are fairly similar. Panel (c) shows that the fixed CDNC for the SB microphysics matches well with the prognostic CDNC from the SALSA simulations. This is the case because total aerosol number was adjusted for this purpose. The most obvious difference is that SIP produces ICNC profiles that have a maximum within the cloud and lower values below while the profiles without SIP are essentially uniform and even increasing with decreasing altitude. The ACLOUD observations cannot show if the profiles should be uniform or not. This is because the observations are subjected to the typical detection limits (cannot see the smallest particles) as well as particle shattering effects (Järvinen et al., 2023), which impacts depend on altitude.

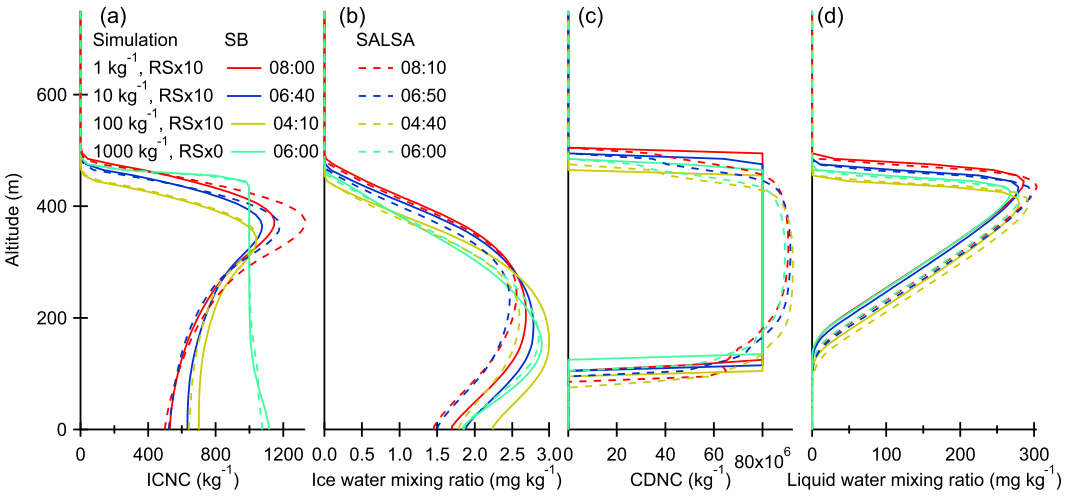

Original Fig. 5.

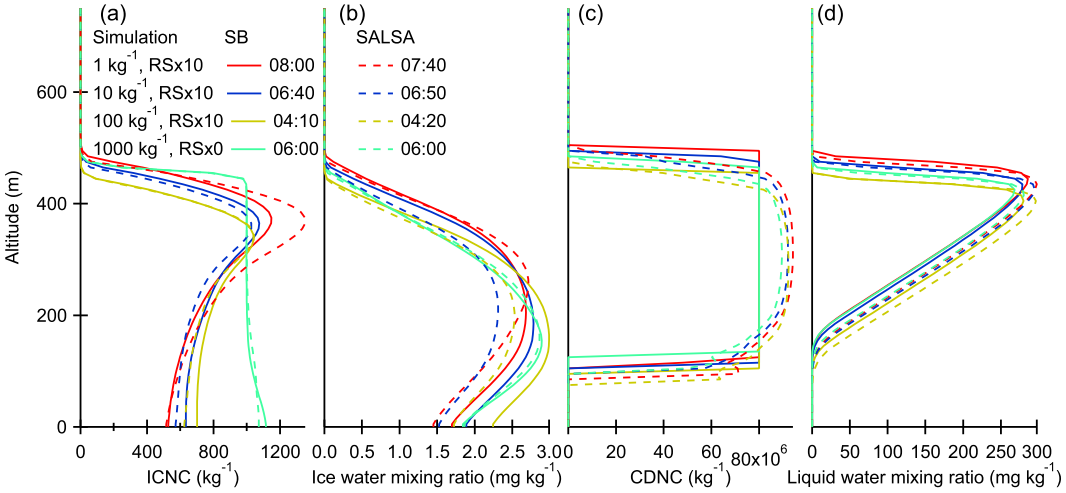

Figure 6. Profiles of (a) ICNC, (b) ice water mixing ratio, (c) CDNC, and (d) liquid water mixing ratio from the different simulations. The time (hh:mm) for each simulation is selected so that ICNC first exceeds $1000\,\mathrm{kg}^{-1}$ at the altitude of $355\,\mathrm{m}$.

Figure 7 shows additional statistics about vertical distributions. Panel (a) shows the minimum absolute temperatures. These and especially their minimum values (cloud top temperatures) are similar for all simulations. Panel (b) show that the parametrized primary ice nucleation takes place mostly at the cloud top, but for the no-SIP simulation ($1000\,\mathrm{kg}^{-1}$, RS$\times$0) the rates are significant for the whole cloud layer. SIP rates are distributed more evenly based on the cloud temperature and liquid water mixing ratio (Fig. 6d). The rime splintering process takes place between 265 and 270 K and the maximum efficiency is at 268 K, which is lower than the minimum cloud top temperatures. In addition, the maximum rate is seen at about 400 m altitude (high liquid water mixing ratios) where the temperatures are about 269 K. This indicates that a cooler temperature profile where the minimum temperature is slightly below 268 K would increase SIP rates. This will be examined in the next section. Due to the different distributions of the primary and secondary ice production, ice crystals in the SIP runs are larger (panel (d)) at the altitudes below the SIP region. There is also a difference between SB and SALSA microphysics so that the mean diameter is larger in SB simulations.

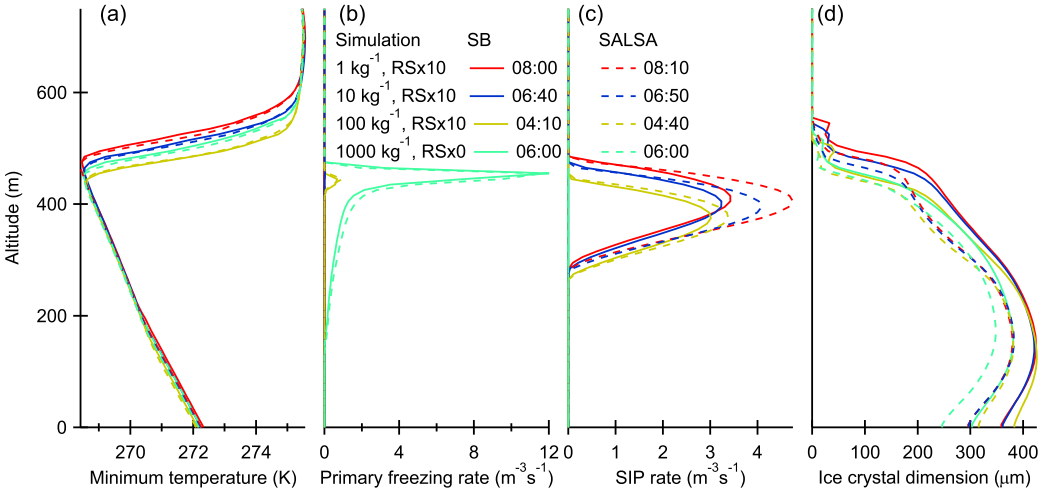

Original Fig. 6.

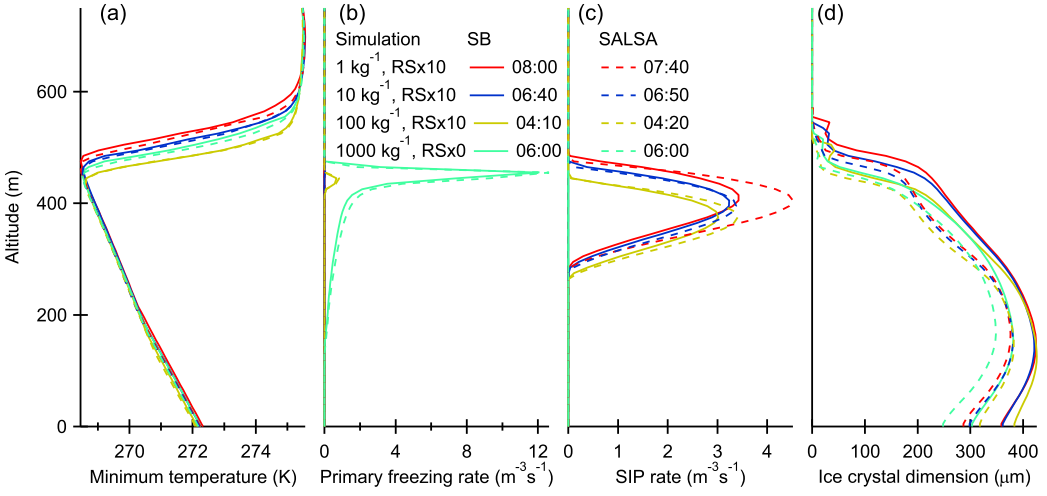

Figure 7. Profiles of (a) minimum absolute temperature, (b) primary freezing rate, (c) RS secondary ice production rate, and (d) ice crystal dimension from the different simulations. The time (hh:mm) for each simulation is selected so that ICNC first exceeds 1000 kg^{-1} at the altitude of 355 m.

3.4 Sensitivity tests

Here we conduct sensitivity tests based on both observational and model variables that are most influential for SIP (see Table A1 for model settings). We use the same approach as above, i.e., determine a multiplier for the SIP rate so that the simulated ice concentration match with reaches the observed ice concentrations concentration of about $1000\,\mathrm{kg}^{-1}$. These simulations are made with the computationally light SB microphysics, because as shown above, SALSA produces qualitatively similar results. We will focus on the case with the highest INP concentration of $100\,\mathrm{kg}^{-1}$ thus the base case simulation has SIP rate multiplied by ten (RS$\times$10). Here we limit simulation time to 10 hours.

The observational variables that will be examined include CDNCand , cloud temperature and water content liquid water path (LWP). Cloud temperature has a direct impact on the rime splintering process while CDNC and LWP have an impact on cloud dynamics. Figure 8 shows how these observational uncertainties influence RS secondary ice production. When simulations are initialized with the humid total water mixing ratio profile (see Fig. 1), LWP is about 30 % higher, but this has a relatively small impact on ice concentration (the **Moist** simulation has the same RS multiplier as in the base casecan be used). The cool profile (θ_L reduced by 2 K), on the other hand, has a clear impact on SIP. Just a factor of two multiplier is enough to start significant ice production in the **Cool** simulation. Initially, the ice concentration increases rapidly but soon the increased precipitation removal starts to limit ice production. Reducing CDNC from $80\times10^6\,\mathrm{kg}^{-1}$ by 50 % to $40\times10^6\,\mathrm{kg}^{-1}$ means that cloud droplets are larger, which means higher fall velocities, so also the riming rate increases. As a result, reducing the multiplier by 40 % from 10 to 6 is enough for the **CDNC/2** simulation to reach and overpass the target ICNC of $1000\,\mathrm{kg}^{-1}$ around the 68$^{\mathrm{th}}$ hour.

Modelling uncertainties are also significant and not only related to the rime splintering parametrization (the number of fragments per accumulated mass of rime, temperature limits, and possible size limits). From the many adjustable model parameters, mass-dimension-velocity (m–D–v) parametrizations seem to have the largest impact on SIP. In Fig. 8, we show simulations where the current ice parametrization is replaced by ice and snow parametrizations from Seifert and Beheng (2006), SB06. The SB06 ice parametrization represents an extreme parametrization regarding ice crystal size, which is increased by almost 100 % (from about 300 to 600 µm). Also, the fall velocity changes, but this has negligible impact on SIP. With this parametrization, SIP becomes more efficient so that a factor of four increase for SIP rate is enough (**SB06 ice *m–D–v***). The SB06 snow parametrization includes the same m–v parametrization as is used for the current ice, so we only change the m–D parametrization which is the same as used by Järvinen et al. (2023) (from Brown and Francis (1995)) for calculating ice mass from the observed ice crystal shapes. This parametrization drastically reduces particle radius from about 300 to 100 µm. This reduced SIP so that it must be multiplied by a factor of 3.5 in addition to the original 10 (**SB06 snow *m–D–v***). The importance of the m–D parametrization can be understood by the fact that collision kernel, which is used for calculating riming rate, is related to the square of the dimension while fall velocity has only linear dependency.

The currently used triangular temperature efficiency curve (linear from zero at 265 K ≈ -8 °C to one at 268 K ≈ -5 °C and back to zero at 270 K ≈ -3 °C) is less efficient compared with some other alternatives. For example, Sotiropoulou et al. (2020) used piecewise constant efficiency curve so that it is one for -6 °C < T < -4 °C and 0.5 for the other temperatures between

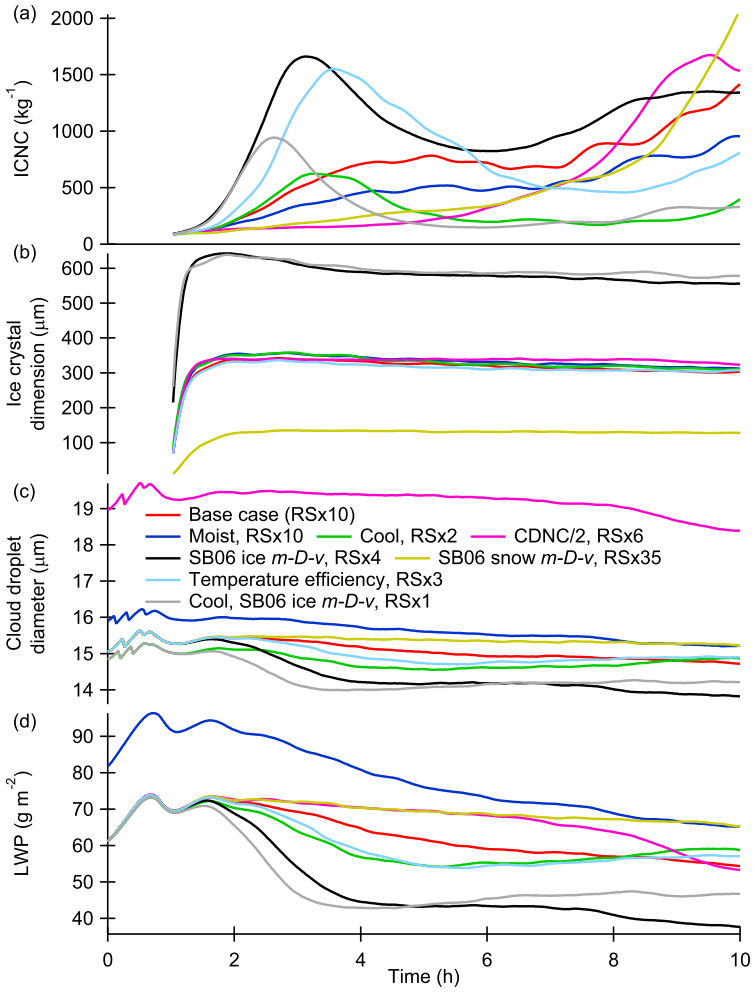

Figure 8. Sensitivity tests based on the observed variability of moisture (Moist), temperature (Cool) and cloud droplet number concentration (CDNC/2), mass-dimension-velocity (m–D–v) parametrizations from Seifert and Beheng (2006) (SB06 ice and snow m–D–v), and temperature efficiency ($f(T)$ in Eq. 1). The last test is with cool profiles and SB06 ice m–D–v parametrization. In each simulation the RS SIP rate is multiplied by a factor so that ice concentration increases to about 1000 kg^{-1}. INP concentration is 100 kg^{-1} in all simulations.

-8 °C < T < -2 °C (Ferrier, 1994). Sullivan et al. (2018b) have unit efficiency between -8 °C < T <-3 °C and 0.01 elsewhere (Takahashi et al., 1995). Ziegler et al. (1986) has parabolic efficiency for temperature range from -2 to -8 °C. As a temperature efficiency test, we modified the efficiency so that it is one between -8 and -3 °C and zero elsewhere. This increases SIP so that only a factor of three increase is needed for the rime splintering (**Temperature efficiency**).

Overall, this sensitivity study suggests that with the cooler temperature profiles, slightly lower CDNC, the ice m–D–v parametrization from SB06, and the more efficient temperature dependency, the LES can reproduce reach the observed ice concentration of about 1000 kg^{-1} without modifying the rime splintering parametrization, and indeed this is the case. This is

shown by the last sensitivity test (**Cool, SB06 ice *m–D–v***) in Fig. 8. Here we have cooler temperature profile and use SB06 ice m–D–v parametrization, but some other combinations of the adjustments would have the same effect.

4 Conclusions

Here we used observations by Järvinen et al. (2023) to initialize LES simulations that aimed at reproducing the high ice concentrations observed in a relatively warm mixed-phase cloud deck where secondary ice production (SIP) was expected to dominate over the primary freezing initiated by INPs. Cloud temperatures were With cloud top temperatures of about -5 °C, so we focused on the dominant SIP process was rime splintering also known as the Hallet-Mossop Hallett-Mossop process. With the default microphysical setup the model was not able to produce secondary ice, even after giving up from the commonly applied size and particle type limitations, so we artificially increased the rime splintering SIP rate by a constant factor. A factor of ten increase was required well enough for the base case so that SIP was able to first rapidly increase the ice crystal number concentration (ICNC) from the primary ice concentration as low as 1 kg^{-1} to the observed above the observed minimum value of about 1000 kg^{-1}, and then maintain that over several hours. Basically this means that a strong enough SIP can become self-sustaining and thus be independent on the primary freezing. Interestingly, the factor of ten increase worked well for the two cloud microphysics models used in this study: the detailed sectional SALSA and the fast two-moment SB (Seifert and Beheng, 2006). The factor of ten happens to be the same enhancement as used in some previous studies (Young et al., 2019; Sotiropoulou et al., 2020; Schäfer et al., 2024).

With the artificially increased the rime splintering SIP rate, SALSA produced steady-state ice concentrations of about 3000 kg^{-1} while this for SB was 2000 kg^{-1}. Although statistically different, the values are surprisingly similar considering the differences between microphysical models and the case where SIP increases ice concentrations by orders of magnitude. Although SB and SALSA produce qualitatively similar results, their computational costs differ a lot. Namely, the computational costs of sectional SALSA microphysics are about 20 times higher than those of the bulk SB microphysics. Here, the efficiency of SB made it useful for conducting large numbers of sensitivity test simulations.

An alternative for artificially adjusting SIP rate is adjusting temperature efficiency or other model parametrizations (mass–dimension–fall velocity) or setup (temperature) to increase SIP. The triangular temperature efficiency curve (linear from zero at 265 K ≈ -8 °C to one at 268 K ≈ -5 °C and back to zero at 270 K ≈ -3 °C) used in the current rime splintering parametrization is less efficient compared with some other alternatives. For example, Sotiropoulou et al. (2020) Sotiropoulou et al. (2020) used piecewise constant efficiency curve so that it is one for -6 °C < T < -4 °C and 0.5 for the other temperatures between -8 °C < T < -2 °C (Ferrier, 1994). Sullivan et al. (2018b) had unit efficiency between -8 °C < T <-3 °C and 0.01 elsewhere (Takahashi et al., 1995). Using any one of these would increase SIP rates. Moisture content has a much smaller effect while cloud droplet number concentration (CDNC) can have a significant effect especially when CDNC is low so that cloud droplets become larger. Mass–dimension–fall velocity parametrizations are important for the riming process, so different parameterisation can either increase or decrease SIP rates. Suitable combination of those can easily initiate self-sustaining secondary ice production even without using any artificial multiplier for the rime splintering rate. On the other hand, defining size or particle

type limits (e.g., excluding ice particles like Kudzotsa et al. (2016), Sullivan et al. (2018a), and Sotiropoulou et al. (2021)) may completely prevent SIP for certain cloud types, especially shallow clouds that have relatively small ice particles and narrow range of in-cloud temperatures. Ideally, such conditions should be replaced by smooth probability terms that reduce ice production in the case of unfavourable conditions. Overall, our results support the previous findings about the high sensitivity of SIP on various model setups and environmental conditions, which is a challenge for modelling.

For the shallow clouds in this study, the other potential SIP mechanism is mechanisms are droplet shattering (DS) based on the temperature range, although large droplets (>30 µm)were not observed (Järvinen et al., 2023). The DS and RS parametrizations share similar features, both being dependent on ice–droplet collisions. For example, Lawson et al. (2015) matched model simulations accounting for droplet shattering to observed ice concentrations by adjusting the number of secondary ice particles produced by per kilogram of accumulated rime mass, which is analogous to the rime splintering parametrization but with different temperature dependency. The optimal value was reported as $10^{-9}\,\mathrm{kg}^{-1}$, but presumably this should be $10^{9}\,\mathrm{kg}^{-1}$, which is about three times larger than the corresponding constant for RSparametrization. However, Lawson et al. (2015) derive this value by assuming that DS is the only SIP process when at least ice-ice collisional breakup would be active at the simulated temperatures between -8 and -20 °C. Due to the similarity, it is not surprising that either DS (Lawson et al., 2015) or RS alone can produce high ice concentrations. This is probably one reason why RS parametrizations are often successfully used as the only SIP parametrization, including this study. It can't be argued that the current RS parametrizations have weaknesses that need to be addressed and that the and ice-ice collisional breakup (IIBR). All SALSA simulations account for DS and IIBR based on parametrizations described in detail by (Calderón et al., 2025), but these SIP processes were at least two orders of magnitude less efficient in producing secondary ice when compared with rime splintering (RS). Clearly, the current shallow cloud with relatively warm temperatures and small droplet sizes is more suitable for RS than for DS or IIBR. It is also clear that other SIP processes (at least droplet shattering and ice-ice collisional breakup) should be accounted for when conditions are more suitable for them. We will focus focused on these processes in another study (Calderón et al., 2025) our previous study (Calderón et al., 2025) on cumulus congestus where cloud temperatures are lower and thus more favourable for them IIBR and DS.

Regardless of the exact mechanism, it is essential to account for SIP rather than fix INP or ice crystal number directly. The simulations showed that vertical ice distributions and ice crystal sizes are different depending on how they were simulated. Moreover, using SIP allows the negative feedback between precipitation and ice production, which allows the development of stable mixed-phase clouds. Increase in the ice concentration will deplete liquid water, which in turn reduces SIP rates and stabilizes the cloud phase partitioning. With high fixed ice concentrations, the clouds are more likely to dissipate or glaciate, which is an issue seen in many large-scale models. Although the simulated vertical ice profiles were different with and without SIP, it was not possible to see if the observations match better with either one of those. However, this could be possible in future studies.

A recent study (Seidel et al., 2024) has questioned the existence of the rime splintering process. Our study cannot confirm that the process is real, but at least the simulated ice concentrations match well with the observed concentrations. The currently (and commonly) used parametrization is simple enough for models that have simplified microphysics (e.g., large-scale models) so it is useful at least for now.

Appendix A: Simulation settings

Figure A1a shows the observed temperatures from three research flights during the warm period and Fig. A1b shows wind speed components from flight 11 (Hartmann et al., 2019). The solid black lines indicate the default LES initialization based on observations from flight 11 (June 2, 2017). The temperature profiles are adiabatic below cloud top and adjusted to match with the observed cloud top temperature and LWP. Adiabatic temperature and cloud water profiles are reconstructed based on given surface temperature and RH. To account for the radiative cooling, the minimum temperature seen at the cloud top is set to be slightly warmer than the observed minimum temperature of -4.56 $^\circ$C. The initial rapid cooling decreases simulated minimum temperatures to -4.5 $^\circ$C and then the cooling continues at a slower rate of -0.03 $^\circ$C/h. LWP is calculated from the cloud water profiles, and to account for the increasing LWP seen in simulations with low ice concentration, the initial value is lower than the observed LWP. The cooler initial profile is reconstructed by reducing surface temperature by 2 K and adjusting surface RH so that LWP is the same as in the default case. The third profile is generated by increasing surface RH so that LWP increases. Overall, these setups cover the observed cloud top temperature and LWP ranges. The initial wind profiles were calculated from the observations as a weighted mean. The weight for altitude x (based on the LES grid) for wind velocity observation at altitude z_i is $w_i(x) = \exp(-((x - z_i)/(50\,\mathrm{m}))^2)$.

Figure A2a shows the observed total aerosol number concentration and Fig. A2b shows the average ambient aerosol size distribution (Mertes et al., 2019). The average aerosol size distribution includes observations from time period 12:12:40 – 12:18:58 when sampling ambient aerosol (marked with the larger dots in panel (a)). The log-normal fit in panel (b) was used to initialize aerosol size distribution for SALSA except that the total aerosol number concentration was set to $150\times10^6\,\mathrm{kg}^{-1}$ ($195\,\mathrm{cm}^{-3}$ when air density is $1.3\,\mathrm{kg\,m}^{-3}$) so that the simulated CDNC matched with the observed value of about $80\times10^6\,\mathrm{kg}^{-1}$.

Table A1 shows the model parameters and settings for all LES simulations. These are also described in the main text.

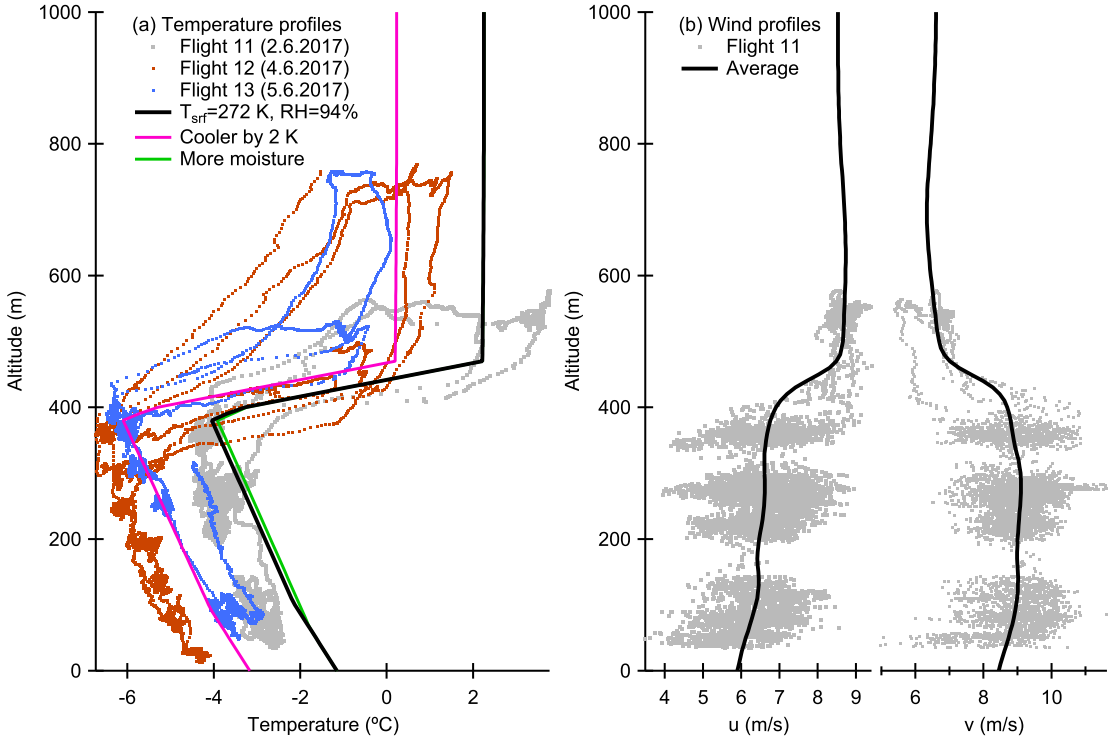

Figure A1. Observed (a) temperature profiles from three research flights during the warm period, and (b) wind profiles for flight 11 (Hartmann et al., 2019). The solid black lines indicate the default LES initialization based on observations from flight 11 (June 2, 2017). The cool and moist temperature profiles are used for additional sensitivity tests described in the main text.

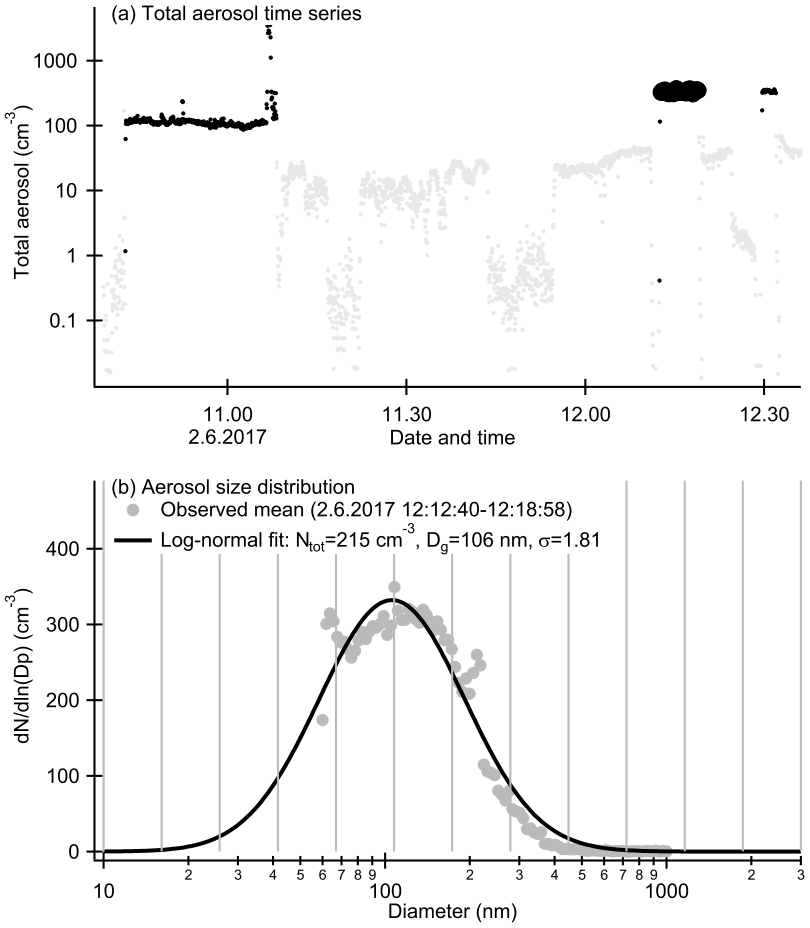

Figure A2. Observed (a) total aerosol number concentration time series and (b) the average ambient aerosol size distribution. The data is from June 2, 2017, flight (Mertes et al., 2019). The black and grey colours in panel (a) indicate time periods when measuring ambient aerosol and cloud particle residuals, respectively. The ambient aerosol size distribution in panel (b) is averaged from time period 12:12:40 – 12:18:58, which is marked with the larger dots in panel (a). Panel (b) also shows a log-normal fit to the data covering the SALSA aerosol bins (bin limits indicated by the grey vertical lines).

Table A1. Model parameters and other simulation settings.

Parameter	Common defaults
Horizontal domain	Nx=Ny=100, dx=dy=100 m
Vertical domain	Nz=85, dz=10 m below 600 m and stretched by 1.03 above that
Time	Maximum step=1 s, total=86400 s, spin-up=3600 s
Outputs	Statistics every 120 s, averages every 600 s
Mean winds	u=9.0 m s^{-1}, v=6.0 m s^{-1}
Θ_{00}	270 K
Four-stream radiation	SZA=60°, background=mid-latitude winter atmosphere (kmlw.lay), α=0.5, SST=272 K
Large-scale divergence	5×10^{-6} s^{-1}
Surface	z_0 = 0.04 m, SHF=0 W m^{-2}, LHF=15 W m^{-2}
Primary ice	Cloud droplets freeze when S_i>0 and ICNC<INP concentration
INP concentrations	1, 10, 100, and 1000 kg^{-1}
RS temperature efficiency	$f(T)$ is linear between T_{min}=265 K, T_{opt} = 268 K, and T_{max} = 270 K
Ice $v = a_v * m^{b_v}$	a_v=27.7, b_v=0.216
Ice $D = a_D * m^{b_D}$	a_D=0.835, b_D=0.390
	SB defaults
Fixed CDNC	80×10^6 kg^{-1}
Riming limits	Droplets: r_c>10^{-6} kg m^{-3}, D_c>10 μm
	Ice: r_i>10^{-9} kg m^{-3}, D_i>0 μm
	SALSA defaults
Initial aerosol	Log-normal size distribution: N_{tot}=150×10^6 kg^{-1}, D_g=0.106 μm, σ=1.81
	Composed of sulfate: M=132.14 g mol^{-1}, ρ = 1770 kg m^{-3}, ν = 2.49
Riming limits	Droplets: N_c>10^{-3} m^{-3}, D_c>10 μm
	Ice: N_i>10^{-6} m^{-3}, D_i>10 μm
Aerosol bins	12 logarithmically spaced bins between 10 and 3000 nm
Rain bins	7 logarithmically spaced bins between 50 and 2000 μm
Ice bins	10 logarithmically spaced bins between 10 and 2000 μm
	Sensitivity tests
Moist	Moist initial profiles
Cool	Cool initial profiles and SST=269.985 K
CDNC/2	CDNC=40×10^6 kg^{-1}
SB06 ice m–D–v	a_v=317, b_v=0.363, a_D=0.217, b_D=0.302
SB06 snow m–D–v	a_v=27.7, b_v=0.216, a_D=8.156, b_D=0.526
RS temperature efficiency	$f(T)$=1 between 265 and 270 K

Code and data availability. Brief description of the simulations, source code of UCLALES-SALSA, and the simulation data used in this publication are available from https://a3s.fi/12001823-acloud-pub/index.html [for review] (Raatikainen, 2026).

Code and data availability. Brief description of the simulations, source code of UCLALES-SALSA, and the simulation data used in this publication are available from https://doi.org/10.5281/zenodo.18184323 (Raatikainen, 2026).

Author contributions. TR designed and conducted UCLALES-SALSA simulations. TR, SC, MP, and SR have contributed to developing the UCLALES-SALSA model. EJ provided the observational data used in this study. TR prepared the manuscript with contributions from all co-authors.

Competing interests. The authors have no competing interests to declare.

Acknowledgements. The authors wish to acknowledge CSC – IT Center for Science, Finland, for computational resources. This research has been supported by the Research Council of Finland (decision numbers 322532 and 359342) and by the European Union's Horizon Europe CleanCloud (grant agreement no. 101137639) and CERTAINTY (no. 101137680) projects.

References

Ackerman, A. S., vanZanten, M. C., Stevens, B., Savic-Jovcic, V., Bretherton, C. S., Chlond, A., Golaz, J.-C., Jiang, H., Khairoutdinov, M., Krueger, S. K., Lewellen, D. C., Lock, A., Moeng, C.-H., Nakamura, K., Petters, M. D., Snider, J. R., Weinbrecht, S., and Zulauf, M.: Large-Eddy Simulations of a Drizzling, Stratocumulus-Topped Marine Boundary Layer, Mon. Weather Rev., 137, 1083 – 1110, https://doi.org/10.1175/2008MWR2582.1, 2009.

Ahola, J., Korhonen, H., Tonttila, J., Romakkaniemi, S., Kokkola, H., and Raatikainen, T.: Modelling mixed-phase clouds with the large-eddy model UCLALES–SALSA, Atmos. Chem. Phys., 20, 11 639–11 654, https://doi.org/10.5194/acp-20-11639-2020, 2020.

Atlas, R. L., Bretherton, C. S., Blossey, P. N., Gettelman, A., Bardeen, C., Lin, P., and Ming, Y.: How Well Do Large-Eddy Simulations and Global Climate Models Represent Observed Boundary Layer Structures and Low Clouds Over the Summertime Southern Ocean?, J. Adv. Model. Earth Sy., 12, e2020MS002 205, https://doi.org/10.1029/2020MS002205, 2020.

Blahak, U.: Towards a better representation of high density ice particles in a state-of-the-art two-moment bulk microphysical scheme, 15th International Conference on Clouds and Precipitation, Cancun, Mexico, July 7-11, 2008, 2008.

Brown, P. R. A. and Francis, P. N.: Improved Measurements of the Ice Water Content in Cirrus Using a Total-Water Probe, J. Atmos. Ocean. Tech., 12, 410 – 414, https://doi.org/10.1175/1520-0426(1995)012<0410:IMOTIW>2.0.CO;2, 1995.

Calderón, S. M., Hyttinen, N., Kokkola, H., Raatikainen, T., Lawson, R. P., and Romakkaniemi, S.: Secondary Ice Formation in Cumulus Congestus Clouds: Insights from Observations and Aerosol-Aware Large-Eddy Simulations, EGUsphere, 2025, 1–33, https://doi.org/10.5194/egusphere-2025-2730ice formation in cumulus congestus clouds: insights from observations and aerosol-aware large-eddy simulations, Atmos. Chem. Phys., 25, 14 479–14 500, https://doi.org/10.5194/acp-25-14479-2025, 2025.

Cesana, G. and Storelvmo, T.: Improving climate projections by understanding how cloud phase affects radiation, J. Geophys. Res.-Atmos., 122, 4594–4599, https://doi.org/10.1002/2017JD026927, 2017.

Cotton, W. R., Tripoli, G. J., Rauber, R. M., and Mulvihill, E. A.: Numerical Simulation of the Effects of Varying Ice Crystal Nucleation Rates and Aggregation Processes on Orographic Snowfall, J. Appl. Meteorol. Climatol., 25, 1658–1680, https://doi.org/10.1175/1520-0450(1986)025<1658:NSOTEO>2.0.CO;2, 1986.

Eirund, G. K., Possner, A., and Lohmann, U.: Response of Arctic mixed-phase clouds to aerosol perturbations under different surface forcings, Atmos. Chem. Phys., 19, 9847–9864, https://doi.org/10.5194/acp-19-9847-2019, 2019.

Ehrlich, A., Wendisch, M., Lüpkes, C., Buschmann, M., Bozem, H., Chechin, D., Clemen, H.-C., Dupuy, R., Eppers, O., Hartmann, J., Herber, A., Jäkel, E., Järvinen, E., Jourdan, O., Kästner, U., Kliesch, L.-L., Köllner, F., Mech, M., Mertes, S., Neuber, R., Ruiz-Donoso, E., Schnaiter, M., Schneider, J., Stapf, J., and Zanatta, M.: A comprehensive in situ and remote sensing data set from the Arctic CLoud Observations Using airborne measurements during polar Day (ACLOUD) campaign, Earth Syst. Sci. Data, 11, 1853–1881, https://doi.org/10.5194/essd-11-1853-2019, 2019.

Ferrier, B. S.: A Double-Moment Multiple-Phase Four-Class Bulk Ice Scheme. Part I: Description, J. Atmos. Sci., 51, 249–280, https://doi.org/10.1175/1520-0469(1994)051<0249:ADMMPF>2.0.CO;2, 1994.

Field, P. R., Lawson, R. P., Brown, P. R. A., Lloyd, G., Westbrook, C., Moisseev, D., Miltenberger, A., Nenes, A., Blyth, A., Choularton, T., Connolly, P., Buehl, J., Crosier, J., Cui, Z., Dearden, C., DeMott, P., Flossmann, A., Heymsfield, A., Huang, Y., Kalesse, H., Kanji, Z. A., Korolev, A., Kirchgaessner, A., Lasher-Trapp, S., Leisner, T., McFarquhar, G., Phillips, V., Stith, J., and Sullivan, S.: Secondary Ice Production: Current State of the Science and Recommendations for the Future, Meteorol. Monogr., 58, 7.1–7.20, https://doi.org/10.1175/AMSMONOGRAPHS-D-16-0014.1, 2017.

Gierens, R., Kneifel, S., Shupe, M. D., Ebell, K., Maturilli, M., and Löhnert, U.: Low-level mixed-phase clouds in a complex Arctic environment, Atmos. Chem. Phys., 20, 3459–3481, https://doi.org/10.5194/acp-20-3459-2020, 2020.

Grzegorczyk, P., Wobrock, W., Canzi, A., Niquet, L., Tridon, F., and Planche, C.: Investigating secondary ice production in a deep convective cloud with a 3D bin microphysics model: Part I – Sensitivity study of microphysical processes representations, Atmos. Res., 313, 107774, https://doi.org/10.1016/j.atmosres.2024.107774, 2025.

Hallett, J. and Mossop, S. C.: Production of secondary ice particles during the riming process, Nature, 249, 26–28, https://doi.org/10.1038/249026a0, 1974.

Hartmann, J., Lüpkes, C., and Chechin, D.: 1Hz resolution aircraft measurements of wind and temperature during the ACLOUD campaign in 2017, https://doi.org/10.1594/PANGAEA.902849, 2019.

Hohenegger, C., Korn, P., Linardakis, L., Redler, R., Schnur, R., Adamidis, P., Bao, J., Bastin, S., Behravesh, M., Bergemann, M., Biercamp, J., Bockelmann, H., Brokopf, R., Brüggemann, N., Casaroli, L., Chegini, F., Datseris, G., Esch, M., George, G., Giorgetta, M., Gutjahr, O., Haak, H., Hanke, M., Ilyina, T., Jahns, T., Jungclaus, J., Kern, M., Klocke, D., Kluft, L., Kölling, T., Kornblueh, L., Kosukhin, S., Kroll, C., Lee, J., Mauritsen, T., Mehlmann, C., Mieslinger, T., Naumann, A. K., Paccini, L., Peinado, A., Praturi, D. S., Putrasahan, D., Rast, S., Riddick, T., Roeber, N., Schmidt, H., Schulzweida, U., Schütte, F., Segura, H., Shevchenko, R., Singh, V., Specht, M., Stephan, C. C., von Storch, J.-S., Vogel, R., Wengel, C., Winkler, M., Ziemen, F., Marotzke, J., and Stevens, B.: ICON-Sapphire: simulating the components of the Earth system and their interactions at kilometer and subkilometer scales, Geosci. Model Dev., 16, 779–811, https://doi.org/10.5194/gmd-16-779-2023, 2023.

Huang, Y., Blyth, A. M., Brown, P. R. A., Choularton, T. W., Connolly, P., Gadian, A. M., Jones, H., Latham, J., Cui, Z., and Carslaw, K.: The development of ice in a cumulus cloud over southwest England, New J. Phys., 10, 105 021, https://doi.org/10.1088/1367-2630/10/10/105021, 2008.

Järvinen, E., Nehlert, F., Xu, G., Waitz, F., Mioche, G., Dupuy, R., Jourdan, O., and Schnaiter, M.: Investigating the vertical extent and short-wave radiative effects of the ice phase in Arctic summertime low-level clouds, Atmos. Chem. Phys., 23, 7611–7633, https://doi.org/10.5194/acp-23-7611-2023, 2023.

Kanji, Z. A., Ladino, L. A., Wex, H., Boose, Y., Burkert-Kohn, M., Cziczo, D. J., and Krämer, M.: Overview of Ice Nucleating Particles, Meteor. Mon., 58, 1.1–1.33, https://doi.org/10.1175/AMSMONOGRAPHS-D-16-0006.1, 2017.

Keinert, A., Spannagel, D., Leisner, T., and Kiselev, A.: Secondary Ice Production upon Freezing of Freely Falling Drizzle Droplets, J. Atmos. Sci., 77, 2959–2967, https://doi.org/10.1175/JAS-D-20-0081.1, 2020.

Korolev, A., McFarquhar, G., Field, P. R., Franklin, C., Lawson, P., Wang, Z., Williams, E., Abel, S. J., Axisa, D., Borrmann, S., Crosier, J., Fugal, J., Krämer, M., Lohmann, U., Schlenczek, O., Schnaiter, M., and Wendisch, M.: Mixed-Phase Clouds: Progress and Challenges, Meteor. Mon., 58, 5.1–5.50, https://doi.org/10.1175/AMSMONOGRAPHS-D-17-0001.1, 2017.

Kudzotsa, I., Phillips, V. T. J., Dobbie, S., Formenton, M., Sun, J., Allen, G., Bansemer, A., Spracklen, D., and Pringle, K.: Aerosol indirect effects on glaciated clouds. Part I: Model description, Q. J. Roy. Meteor. Soc., 142, 1958–1969, https://doi.org/10.1002/qj.2791, 2016.

Lawson, R. P., Woods, S., and Morrison, H.: The Microphysics of Ice and Precipitation Development in Tropical Cumulus Clouds, J. Atmos. Sci., 72, 2429–2445, https://doi.org/10.1175/JAS-D-14-0274.1, 2015.

Li, G., Wieder, J., Pasquier, J. T., Henneberger, J., and Kanji, Z. A.: Predicting atmospheric background number concentration of ice-nucleating particles in the Arctic, Atmos. Chem. Phys., 22, 14 441–14 454, https://doi.org/10.5194/acp-22-14441-2022, 2022.

Listowski, C., Delanoë, J., Kirchgaessner, A., Lachlan-Cope, T., and King, J.: Antarctic clouds, supercooled liquid water and mixed phase, investigated with DARDAR: geographical and seasonal variations, Atmos. Chem. Phys., 19, 6771–6808, https://doi.org/10.5194/acp-19-6771-2019, 2019.

Luke, E. P., Yang, F., Kollias, P., Vogelmann, A. M., and Maahn, M.: New insights into ice multiplication using remote-sensing observations of slightly supercooled mixed-phase clouds in the Arctic, P. Natl. Acad. Sci. USA, 118, e2021387 118, https://doi.org/10.1073/pnas.2021387118, 2021.

McFarquhar, G. M. and Cober, S. G.: Single-Scattering Properties of Mixed-Phase Arctic Clouds at Solar Wavelengths: Impacts on Radiative Transfer, J. Clim., 17, 3799–3813, https://doi.org/10.1175/1520-0442(2004)017<3799:SPOMAC>2.0.CO;2, 2004.

Mertes, S., Kästner, U., and Macke, A.: Airborne in-situ measurements of the aerosol absorption coefficient, aerosol particle number concentration and size distribution of cloud particle residuals and ambient aerosol particles during flight P6_206_ACLOUD_2017_1706021001, PANGAEA, https://doi.org/10.1594/PANGAEA.900414, in: Mertes, S et al. (2019): Airborne in-situ measurements of the aerosol absorption coefficient, aerosol particle number concentration and size distribution of cloud particle residuals and ambient aerosol particles during the ACLOUD campaign in May and June 2017 [dataset publication series]. Leibniz-Institut für Troposphärenforschung e.V., Leipzig, PANGAEA, https://doi.org/10.1594/PANGAEA.900403, 2019.

Mioche, G., Jourdan, O., Ceccaldi, M., and Delanoë, J.: Variability of mixed-phase clouds in the Arctic with a focus on the Svalbard region: a study based on spaceborne active remote sensing, Atmos. Chem. Phys., 15, 2445–2461, https://doi.org/10.5194/acp-15-2445-2015, 2015.

Mioche, G., Jourdan, O., Delanoë, J., Gourbeyre, C., Febvre, G., Dupuy, R., Monier, M., Szczap, F., Schwarzenboeck, A., and Gayet, J.-F.: Vertical distribution of microphysical properties of Arctic springtime low-level mixed-phase clouds over the Greenland and Norwegian seas, Atmos. Chem. Phys., 17, 12 845–12 869, https://doi.org/10.5194/acp-17-12845-2017, 2017.

Morrison, H., Thompson, G., and Tatarskii, V.: Impact of Cloud Microphysics on the Development of Trailing Stratiform Precipitation in a Simulated Squall Line: Comparison of One- and Two-Moment Schemes, Mon. Weather Rev., 137, 991–1007, https://doi.org/10.1175/2008MWR2556.1, 2009.

Murray, B. J., Carslaw, K. S., and Field, P. R.: Opinion: Cloud-phase climate feedback and the importance of ice-nucleating particles, Atmos. Chem. Phys., 21, 665–679, https://doi.org/10.5194/acp-21-665-2021, 2021.

Noppel, H., Blahak, U., Seifert, A., and Beheng, K. D.: Simulations of a hailstorm and the impact of CCN using an advanced two-moment cloud microphysical scheme, Atmos. Res., 96, 286–301, https://doi.org/10.1016/j.atmosres.2009.09.008, 15th International Conference on Clouds and Precipitation, 2010.

Pasquier, J. T., Henneberger, J., Ramelli, F., Lauber, A., David, R. O., Wieder, J., Carlsen, T., Gierens, R., Maturilli, M., and Lohmann, U.: Conditions favorable for secondary ice production in Arctic mixed-phase clouds, Atmos. Chem. Phys., 22, 15 579–15 601, https://doi.org/10.5194/acp-22-15579-2022, 2022.

Petters, M. D. and Kreidenweis, S. M.: A single parameter representation of hygroscopic growth and cloud condensation nucleus activity, Atmos. Chem. Phys., 7, 1961–1971, https://doi.org/10.5194/acp-7-1961-2007, 2007.

Phillips, V. T. J., Yano, J.-I., and Khain, A.: Ice Multiplication by Breakup in Ice–Ice Collisions. Part I: Theoretical Formulation, J. Atmos. Sci., 74, 1705–1719, https://doi.org/10.1175/JAS-D-16-0224.1, 2017.

Phillips, V. T. J., Patade, S., Gutierrez, J., and Bansemer, A.: Secondary Ice Production by Fragmentation of Freezing Drops: Formulation and Theory, J. Atmos. Sci., 75, 3031–3070, https://doi.org/10.1175/JAS-D-17-0190.1, 2018.

Prenni, A. J., Harrington, J. Y., Tjernström, M., DeMott, P. J., Avramov, A., Long, C. N., Kreidenweis, S. M., Olsson, P. Q., and Verlinde, J.: Can Ice-Nucleating Aerosols Affect Arctic Seasonal Climate?, Bull. Amer. Meteor. Soc., 88, 541–550, https://doi.org/10.1175/BAMS-88-4-541, 2007.

Previdi, M., Smith, K. L., and Polvani, L. M.: Arctic amplification of climate change: a review of underlying mechanisms, Environ. Res. Lett., 16, 093003, https://doi.org/10.1088/1748-9326/ac1c29, 2021.

Raatikainen, T.: UCLALES-SALSA simulations for the ACLOUD campaign, Finnish Meteorological Institute Code and data for "Can rime splintering explain the ice production in Arctic mixed-phase clouds?" , Zenodo [data set] https://a3s.fi/12001823-acloud-pub/index.html, 2025. https://doi.org/10.5281/zenodo.18184323, 2026.

Rangno, A. L. and Hobbs, P. V.: Ice particles in stratiform clouds in the Arctic and possible mechanisms for the production of high ice concentrations, J. Geophys. Res.-Atmos., 106, 15 065–15 075, https://doi.org/https://doi.org/10.1029/2000JD900286, 2001.

Reisner, J., Rasmussen, R. M., and Bruintjes, R. T.: Explicit forecasting of supercooled liquid water in winter storms using the MM5 mesoscale model, Q. J. Roy. Meteor. Soc., 124, 1071–1107, https://doi.org/10.1002/qj.49712454804, 1998.

Schäfer, B., David, R. O., Georgakaki, P., Pasquier, J. T., Sotiropoulou, G., and Storelvmo, T.: Simulations of primary and secondary ice production during an Arctic mixed-phase cloud case from the Ny-Ålesund Aerosol Cloud Experiment (NASCENT) campaign, Atmos. Chem. Phys., 24, 7179–7202, https://doi.org/10.5194/acp-24-7179-2024, 2024.

Seidel, J. S., Kiselev, A. A., Keinert, A., Stratmann, F., Leisner, T., and Hartmann, S.: Secondary ice production – no evidence of efficient rime-splintering mechanism, Atmos. Chem. Phys., 24, 5247–5263, https://doi.org/10.5194/acp-24-5247-2024, 2024.

Seifert, A.: On the Parameterization of Evaporation of Raindrops as Simulated by a One-Dimensional Rainshaft Model, J. Atmos. Sci., 65, 3608–3619, https://doi.org/10.1175/2008JAS2586.1, 2008.

Seifert, A. and Beheng, K. D.: A double-moment parameterization for simulating autoconversion, accretion and selfcollection, Atmos. Res., 59–60, 265–281, https://doi.org/10.1016/S0169-8095(01)00126-0, 13th International Conference on Clouds and Precipitation, 2001.

Seifert, A. and Beheng, K. D.: A two-moment cloud microphysics parameterization for mixed-phase clouds. Part 1: Model description, Meteorol. Atmos. Phys., 92, 45–66, https://doi.org/10.1007/s00703-005-0112-4, 2006.

Seifert, A. and Heus, T.: Large-eddy simulation of organized precipitating trade wind cumulus clouds, Atmos. Chem. Phys., 13, 5631–5645, https://doi.org/10.5194/acp-13-5631-2013, 2013.

Seifert, A., Köhler, C., and Beheng, K. D.: Aerosol-cloud-precipitation effects over Germany as simulated by a convective-scale numerical weather prediction model, Atmos. Chem. Phys., 12, 709–725, https://doi.org/10.5194/acp-12-709-2012, 2012.

Seifert, A., Blahak, U., and Buhr, R.: On the analytic approximation of bulk collision rates of non-spherical hydrometeors, Geosci. Model Dev., 7, 463–478, https://doi.org/10.5194/gmd-7-463-2014, 2014.

Sotiropoulou, G., Sullivan, S., Savre, J., Lloyd, G., Lachlan-Cope, T., Ekman, A. M. L., and Nenes, A.: The impact of secondary ice production on Arctic stratocumulus, Atmos. Chem. Phys., 20, 1301–1316, https://doi.org/10.5194/acp-20-1301-2020, 2020.

Sotiropoulou, G., Vignon, E., Young, G., Morrison, H., O'Shea, S. J., Lachlan-Cope, T., Berne, A., and Nenes, A.: Secondary ice production in summer clouds over the Antarctic coast: an underappreciated process in atmospheric models, Atmos. Chem. Phys., 21, 755–771, https://doi.org/10.5194/acp-21-755-2021, 2021.

Stevens, B. and Seifert, A.: Understanding macrophysical outcomes of microphysical choices in simulations of shallow cumulus convection, J. Meteorol. Soc. Jpn. Ser. II, 86A, 143–162, https://doi.org/10.2151/jmsj.86A.143, 2008.

Stevens, B., Moeng, C.-H., and Sullivan, P. P.: Large-Eddy Simulations of Radiatively Driven Convection: Sensitivities to the Representation of Small Scales, J. Atmos. Sci., 56, 3963–3984, https://doi.org/10.1175/1520-0469(1999)056<3963:LESORD>2.0.CO;2, 1999.

Stevens, B., Moeng, C.-H., Ackerman, A. S., Bretherton, C. S., Chlond, A., de Roode, S., Edwards, J., Golaz, J.-C., Jiang, H., Khairoutdinov, M., Kirkpatrick, M. P., Lewellen, D. C., Lock, A., Müller, F., Stevens, D. E., Whelan, E., and Zhu, P.: Evaluation of Large-Eddy Simulations via Observations of Nocturnal Marine Stratocumulus, Mon. Weather Rev., 133, 1443–1462, https://doi.org/10.1175/MWR2930.1, 2005.

Sullivan, S. C., Hoose, C., and Nenes, A.: Investigating the contribution of secondary ice production to in-cloud ice crystal numbers, J. Geophys. Res.-Atmos., 122, 9391–9412, https://doi.org/10.1002/2017JD026546, 2017.

Sullivan, S. C., Barthlott, C., Crosier, J., Zhukov, I., Nenes, A., and Hoose, C.: The effect of secondary ice production parameterization on the simulation of a cold frontal rainband, Atmos. Chem. Phys., 18, 16 461–16 480, https://doi.org/10.5194/acp-18-16461-2018, 2018a.

Sullivan, S. C., Hoose, C., Kiselev, A., Leisner, T., and Nenes, A.: Initiation of secondary ice production in clouds, Atmos. Chem. Phys., 18, 1593–1610, https://doi.org/10.5194/acp-18-1593-2018, 2018b.

Takahashi, T., Nagao, Y., and Kushiyama, Y.: Possible High Ice Particle Production during Graupel–Graupel Collisions, J. Atmos. Sci., 52, 4523–4527, https://doi.org/10.1175/1520-0469(1995)052<4523:PHIPPD>2.0.CO;2, 1995.

Tonttila, J., Maalick, Z., Raatikainen, T., Kokkola, H., Kühn, T., and Romakkaniemi, S.: UCLALES–SALSA v1.0: a large-eddy model with interactive sectional microphysics for aerosol, clouds and precipitation, Geosci. Model Dev., 10, 169–188, https://doi.org/10.5194/gmd-10-169-2017, 2017.

Tonttila, J., Afzalifar, A., Kokkola, H., Raatikainen, T., Korhonen, H., and Romakkaniemi, S.: Precipitation enhancement in stratocumulus clouds through airborne seeding: sensitivity analysis by UCLALES-SALSA, Atmos. Chem. Phys., 21, 1035–1048, https://doi.org/10.5194/acp-21-1035-2021, 2021.

van der Dussen, J. J., de Roode, S. R., Ackerman, A. S., Blossey, P. N., Bretherton, C. S., Kurowski, M. J., Lock, A. P., Neggers, R. A. J., Sandu, I., and Siebesma, A. P.: The GASS/EUCLIPSE model intercomparison of the stratocumulus transition as observed during ASTEX: LES results, J. Adv. Model. Earth Sy., 5, 483–499, https://doi.org/10.1002/jame.20033, 2013.

Weiss, A. I., King, J., Lachlan-Cope, T., and Ladkin, R.: On the effective aerodynamic and scalar roughness length of Weddell Sea ice, J. Geophys. Res.-Atmos., 116, https://doi.org/10.1029/2011JD015949, 2011.

Wendisch, M., Macke, A., Ehrlich, A., Lüpkes, C., Mech, M., Chechin, D., Dethloff, K., Velasco, C. B., Bozem, H., Brückner, M., Clemen, H.-C., Crewell, S., Donth, T., Dupuy, R., Ebell, K., Egerer, U., Engelmann, R., Engler, C., Eppers, O., Gehrmann, M., Gong, X., Gottschalk, M., Gourbeyre, C., Griesche, H., Hartmann, J., Hartmann, M., Heinold, B., Herber, A., Herrmann, H., Heygster, G., Hoor, P., Jafariserajehlou, S., Jäkel, E., Järvinen, E., Jourdan, O., Kästner, U., Kecorius, S., Knudsen, E. M., Köllner, F., Kretzschmar, J., Lelli, L., Leroy, D., Maturilli, M., Mei, L., Mertes, S., Mioche, G., Neuber, R., Nicolaus, M., Nomokonova, T., Notholt, J., Palm, M., van Pinxteren, M., Quaas, J., Richter, P., Ruiz-Donoso, E., Schäfer, M., Schmieder, K., Schnaiter, M., Schneider, J., Schwarzenböck, A., Seifert, P., Shupe, M. D., Siebert, H., Spreen, G., Stapf, J., Stratmann, F., Vogl, T., Welti, A., Wex, H., Wiedensohler, A., Zanatta, M., and Zeppenfeld, S.: The Arctic Cloud Puzzle: Using ACLOUD/PASCAL Multiplatform Observations to Unravel the Role of Clouds and Aerosol Particles in Arctic Amplification, Bull. Amer. Meteor. Soc., 100, 841–871, https://doi.org/10.1175/BAMS-D-18-0072.1, 2019.

Young, G., Jones, H. M., Choularton, T. W., Crosier, J., Bower, K. N., Gallagher, M. W., Davies, R. S., Renfrew, I. A., Elvidge, A. D., Darbyshire, E., Marenco, F., Brown, P. R. A., Ricketts, H. M. A., Connolly, P. J., Lloyd, G., Williams, P. I., Allan, J. D., Taylor, J. W., Liu, D., and Flynn, M. J.: Observed microphysical changes in Arctic mixed-phase clouds when transitioning from sea ice to open ocean, Atmos. Chem. Phys., 16, 13 945–13 967, https://doi.org/10.5194/acp-16-13945-2016, 2016.

Young, G., Lachlan-Cope, T., O'Shea, S. J., Dearden, C., Listowski, C., Bower, K. N., Choularton, T. W., and Gallagher, M. W.: Radiative Effects of Secondary Ice Enhancement in Coastal Antarctic Clouds, Geophys. Res. Lett., 46, 2312–2321, https://doi.org/10.1029/2018GL080551, 2019.

Zhao, X., Liu, X., Phillips, V. T. J., and Patade, S.: Impacts of secondary ice production on Arctic mixed-phase clouds based on ARM observations and CAM6 single-column model simulations, Atmos. Chem. Phys., 21, 5685–5703, https://doi.org/10.5194/acp-21-5685-2021, 2021.

Ziegler, C. L., Ray, P. S., and MacGorman, D. R.: Relations of Kinematics, Microphysics and Electrification in an Isolated Mountain Thunderstorm, J. Atmos. Sci., 43, 2098–2115, https://doi.org/10.1175/1520-0469(1986)043<2098:ROKMAE>2.0.CO;2, 1986.